REPUBLIC OF TURKEY

ADANA ALPARSLAN TÜRKEŞ SCIENCE AND TECHNOLOGY UNIVERSITY

GRADUATE SCHOOL
BIOENGINEERING DEPARTMENT

MOLECULAR MODELING OF BIO-MOFs FOR ANESTHETIC Xe RECOVERY FROM EXHALE GAS MIXTURES

BEHRA CANTÜRK

M.Sc.

ADANA 2023

REPUBLIC OF TURKEY

ADANA ALPARSLAN TÜRKEŞ SCIENCE AND TECHNOLOGY UNIVERSITY

GRADUATE SCHOOL
BIOENGINEERING DEPARTMENT

MOLECULAR MODELING OF BIO-MOFs FOR ANESTHETIC Xe RECOVERY FROM EXHALE GAS MIXTURES

BEHRA CANTÜRK

M.Sc.

THESIS ADVISOR
Assoc. Prof. Dr. YELİZ GÜRDAL DURĞUN

ADANA, YEAR 2023

DECLARATION OF CONFORMITY

In this thesis study, which was prepared following the thesis writing rules of Adana Alparslan Türkeş Science and Technology University Institute of Graduate School, I declare that I provide all the information, documents, evaluations and results in accordance with scientific ethics and moral codes without resorting to any means or assistance that would be contrary to scientific ethics and traditions. I also declare that I refer to all of the articles I used in this study with appropriate references and accept all moral and legal consequences if a situation is found contrary to my statement regarding my work.

09/12/2022

Behra CANTÜRK

ÖZET

Bio-MOF'lar Kullanılarak Ekshale Gaz Karışımlarından Anestezik Xe Geri Kazanımının Moleküler Modellenmesi

Behra CANTÜRK
Yüksek Lisans, Biyomühendislik Anabilim Dalı
Danışman: Doç. Dr. Yeliz GÜRDAL DURĞUN
Aralık 2022, 60 sayfa

Xenon (Xe) için ucuz ve verimli bir geri kazanım süreci tasarlamak, sürdürülebilir uygulamaların geliştirilmesinde önem kazanmaktadır. Xe'yi anestezik gaz karışımlarından ayırmak için metal organik çerçevelerin (MOF'lar) kullanılması, literatürde nadiren ve yüzeysel olarak incelenen bir konudur. Bu tezde, biyo-uyumlu metal katyonlar ve biyolojik bağlayıcılar tarafından oluşturulan 43 biyolojik MOF'un (Bio-MOF) Xe geri kazanım performansları teorik olarak araştırılmıştır. CO_2, O_2 ve N_2 ile ikili karışımlarındaki Xe alımları ve Xe geçirgenlikleri, Grand Canonical Monte Carlo ve Molecular Dynamics simülasyonları uygulanarak hesaplanmıştır. Metaloporfirin, hekzakarboksilat, triazin veya pirazol ligandları, dimetalik birimleri, nispeten büyük gözenek boyutları (PLD>5 Å ve LCD>10 Å), boşluk fraksiyonları (≈0,8) ve geniş yüzey alanları (>2900 m^2/g) içeren malzemeler Xe geri kazanımı için en yüksek performanslı Bio-MOF'lar olarak belirlenmiştir. Sonuçlarımız, Xe'nin nanogözenekli malzemelerdeki seçici adsorpsiyonunda kritik bir rol oynayan, nadiren incelenen aerojen etkileşimlerinin örneklerini göstermektedir.

Anahtar Kelimeler: B Grand Kanonik Monte Carlo, Molekuler Dinamik, Xenon, Biyolojik MOF.

ABSTRACT

Molecular Modeling Of Bio-MOFs For Anesthetic Xe Recovery From Exhale Gas Mixtures

Behra CANTÜRK
M.Sc., Department of Bioengineering

Supervisor: Assoc. Prof. Dr. Yeliz GÜRDAL DURĞUN
December 2022, 60 pages

Designing an in expensive and highly efficient recovery process for Xenon (Xe) is gaining importance in the development of sustainable applications. Using metal organic frameworks (MOFs) for separating Xe from anesthetic gas mixtures has been a recent topic studied rarely and superficially in the literature. In this thesis, we theoretically investigate Xe recovery performances of 43 biological MOFs (Bio-MOFs) formed by biocompatible metal cations and biological endogenous linkers. Xe uptakes and Xe permeabilities in its binary mixtures with CO_2, O_2, and N_2 are investigated by applying Grand Canonical Monte Carlo and Molecular Dynamics simulations. Materials having metalloporphyrin, hexacarboxylate, triazine, or pyrazole ligands, dimetallic paddlewheel units, relatively large pore sizes (PLD>5 Å and LCD>10 Å), large void fractions (≈0.8), and large surface areas (>2900 m^2/g) are determined as top performing Bio-MOFs for Xe recovery. The results of this thesis show examples of rarely studied aerogen interactions that play a critical role in selective adsorption of Xe in nanoporous materials.

Keywords: Grand Canonical Monte Carlo, Molecular Dynamics, Xenon, Biological MOFs.

Dedication

To my beloved mom and father,

Halil- Halime Cantürk

and

Mert Oğuzhan Oğuz

for always standing behind me with their love and support.

ACKNOWLEDGEMENTS

During my graduate studies, I had the opportunity to meet many excellent people. I would like to express my sincere thanks to each of them in these lines, in my native language. First of all, I would like to thank my esteemed teacher, Associate Professor Yeliz Gürdal, who is my thesis advisor. I have the honor of being one of her first students. I learned a lot from her during the two years we spent together. She was always ready to help me with her understanding, smiling and sincere demeanor. I hope you will always be with me. I would like to thank you for being with me both with your ideas and with your sincere attitude during my graduate process. I am very lucky to be part of the Molecular Modeling team. It's been so long that it makes me sad to be leaving now. With the inspiration I get from you, I can't wait to continue on my way and train myself. I would like to state that it is an honor for me to develop every teaching we have learned from you and to receive this flag from you. I would like to thank Zekiye Erarslan and Gülay Akköse, for whom we struggled together in every issue and who did not leave me alone in this difficult process.

I would like to express my gratitude for being by my side during this process, and of course I owe my family a debt of gratitude as well. My dear family deserves the biggest thanks for always believing in me. I am so happy that they truly support me and are always there for me. I will always work hard to be someone they can be proud of.

I would like to acknowledge the Scientific and Technological Research Council of Turkey (TUBITAK). This study has received funding from the TUBITAK under the 1002 Short Term R&D Funding Program (grant agreement No: 120Z160). The numerical calculations in this research were partially made using the resources of TÜBİTAK ULAKBİM, High Performance and Grid Computing Center (TRUBA).

This thesis was supported by TUBITAK under the 1002 Short Term R&D Funding Program with project number 120Z160.

TABLE OF CONTENTS

LIST OF FIGURES

LIST OF TABLES

LIST OF ABBREVIATIONS

N	: Nitrogen
Xe	: Xenon
O	: Oxygen
GCMC	: Grand Canonical Monte Carlo
MD	: Molecular Dynamic
MOF	: Metal Organic Framework
CO_2	: Carbone dioxide

LIST OF SYMBOLS

ε	: energy
k_B	: Boltzmann constant
ϕ	: fractional porasity
c	: concentration
p	: probability of a system in an i th state
p	: momenta of particles
P	: permeability
q	: molecular partition function
r	: coordination of particles
$S_{permeation}$	: permeation selectivity
$S_{adsorption}$	: adsorption selectivity
$S_{diffusion}$	: diffusion selectivity
t	: time
T	: temperature
Wt	: weight
D_s/D_{self}	: self-diffusivity
m	: mass of a particle
K	: Kelvin
S_{ads}	: Selectivity adsorption
V_{MOF}	: volume of a MOF
μ	: chemical potential
U	: energy
GCMC	: Grand Conanical Monte Carlo
MD	: Molecular Dynamic

1. INTRODUCTION

Noble gases have the potential to be used in many engineering and clinical applications due to their low chemical activity, low solubility, low conductivity, low melting and boiling point, high stability, and low ammability. Xenon (Xe), which is a noble gas, has applications such as lighting, biomedical imaging, nuclear magnetic resonance(Banerjee et al. 2018). It has been shown in the literature that Xe can be used as an anesthetic in clinical applications in addition to its applications in engineering (Goto 2002) Xe, indeed, can be used as an anesthetic gas since it has a highly stable structure, low solubility in blood, minimal side effects that can enhance respiration, and it has very low interaction with drug molecules(Sanders, Franks, and Maze 2003). Clinical trials have shown that induction (providing anesthetic depth) and recovery (waking up after anesthesia) are faster when Xe is used as an anesthetic with respect to the generally used nitrousoxide/sevourane or nitrousoxide/isourane anesthesia. In addition to its clinical effects on patients, the use of Xe as an anesthetic is also an advantage when considering the problems of ozone layer depletion and global warming. It is known that nitrousoxide used as an analgesic in anesthesia has an important role in damaging the ozone layer and creates a greenhouse gas effect about 300 times stronger than carbon dioxide and once released it can stay in nature for 150 years. Widely used anesthetics such as isourane, sevourane, and desurane are in the group of hydrouorocarbons and their global warming potentials calculated for 20 years (GWP) are 1401, 349, and 3714 times greater than the carbon dioxide, respectively (Ryan and Nielsen 2010). As a result, searching for new anesthetics and recommending better and safer anesthetics are important in terms of minimizing post-operative damage, increasing postoperative comfort, as well as decreasing ozone layer depletion, and global warming. MOFs and their composites are also used as new materials in catalysis. MOFs have more advantages over conventional catalysts that are critical to their catalysis. MOFs are known to have rational loading active sites as well as functionalization potentials with heeroatoms that are critical for reactions such as oxidation reduction and CO fixation (Ilknur Erucar 2016). In addition, it is seen that MOFs are used in many studies on gas separation purification processes in the literature.

Metal organic frameworks (MOFs) have been synthesized by combining the advantages of organic and inorganic porous materials and they emerged as a new group of nanoporous

materials. The representation of porous materials are shown in Figure 1.1. Metal ions bound by organic binders are needed to form highly porous networks. The emergence of MOFs was triggered in 1999 by a group of researchers(Li et al. 1999). The crystal structures of thousands of synthesized MOFs have been stored in a large database called the Cambridge Crystallographic Data Center (CCDC) (Groom and Allen 2014). MOFs have been extensively studied in recent years especially for biological as well as gas storage and gas separation applications, see Figure 1.2 (Ma and Zhou 2010).

Figure 1.1. The general classification of porous solids is shown. These; polymers, zeolites and MOFs (Li, Sculley, and Zhou 2012).

Bio-inspired metal organic frameworks (bio-MOFs) are one variant of MOFs. Biological metal organic frameworks (Bio-MOFs) contain biocompatible metal cations and linkers such as amino acids, sugars, and nucleobases. Biological metal organic frameworks (Bio-MOFs) reduce the harmful impact on the environment (Sumida et al. 2012). The materials formed in these studies are called Bio-MOF for short. Bio-MOFs are seen in many fields and studies. These include areas such as biological applications and medical applications. Many studies in these areas are discussed in detail. Bio-MOFs have regular porosity and functionality in

chemical structure. Therefore, it has not been studied only for biomedical applications until now. It has also been studied for gas storage and gas separation (McKinlay et al. 2010).

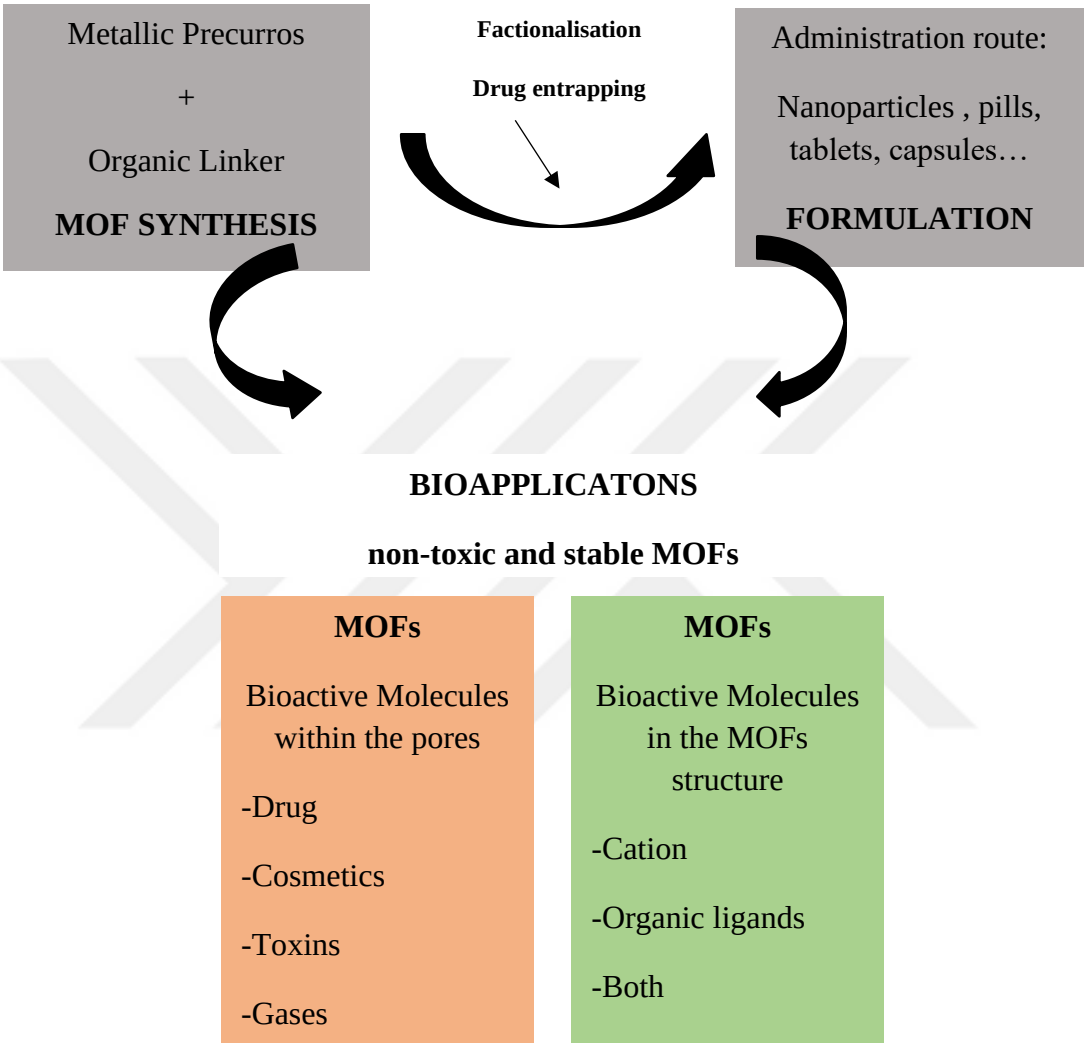

Figure 1.2. Process flow diagram of the MOF manufacturing process for bioapplications (Tamames-Tabar 2014).

Noble gases have properties such as low chemical activity, low solubility, low conductivity, low melting and boiling point, high stability and low flammability . Therefore, they have the potential to be used in many engineering and clinical applications (Banerjee et al. 2018). The noble gas Xenon (Xe) is currently used in applications such as lighting, biomedical imaging, nuclear magnetic resonance (Banerjee et al. 2018) It has been shown in the literature that Xe can be used as an anesthetic in clinical applications in addition to it is applications in the field

of engineering (Ullmann 2003). Today, gas mixtures such as N_2O/sevoflurane and N_2O/isoflurane are used as anesthetics. However it is important to recommend better and safer anesthetics in order to minimize postoperative damages and even deaths and increase postoperative comfort (Stanley 2000).

1.1. **The importance of Xe gas in anesthesia**

Xe can, indeed, be used as an anesthetic gas due to its highly stable structure and low solubility in blood (Sanders et al. 2003). It also has low interaction with drug molecules which results in minimal side effects and improved breathing (Sanders et al. 2003). Anesthetic gases frequently used today are N_2O sevoflurane and desflurane which have blood/gas partition coefficients as 0.47, 0.65, and 0.42, respectively. Xe, on the other hand, has the lowest blood / gas partition coefficient of 0.115 among the commonly used anesthetics (Sanders et al. 2003). Therefore, in cases where Xe is used as an anesthetic, induction (providing anesthetic depth) and recovery (awakening after anesthesia) are reported to be faster (Sanders et al. 2003). It has been shown that recovery is achieved 3 times faster and more smoothly in Xe anesthesia with respect to the conventional anesthetics (Goto 2002). Anesthetics such as sevoflurane and desflurane used today do not have an analgesic effect during surgery. Therefore, anesthetics should be given with pain relievers (analgesic drugs) such as N_2O. On the other hand, Xe has been shown to be both anesthetic and pain reliever (Lynch et al. 2000). Xe is used only with O_2 gas during anesthesia. The minimum alveolar concentration (MAC) values are reported as 72 for Xe and 104 for N_2O (Nickalls and Mapleson 2003), thus Xe gas is, indeed, a stronger anesthetic and pain reliever than N_2O (Nickalls and Mapleson 2003). In addition, studies examining the use of Xe as an anesthetic have shown that it has minimal effect on the cardiovascular system (Lynch et al. 2000). Therefore, the use of Xe as an anesthetic will also be useful in situations where cardiovascular stability must be preserved (Lynch et al. 2000).

Xe does not have chemical activity under normal conditions, thus it can not form covalent bonds with other molecules. However, its wide electron shell can be polarized. It can also interact through induced dipole interactions with nearby molecules (Lynch et al. 2000). It can bind to proteins such as myoglobins or lipids by polarization of electrons (Lynch et al. 2000). Some experimental studies have shown that Xe can have an anesthetic effect as it mediates the inhibition of N-methyl-D-aspartate receptors (Franks et al. 1998).

No mutagenic or carcinogenic effects have been observed in studies investigating the toxicity of Xe anesthesia (Burov et al. 1999). The use of Xe as an anesthetic was approved in Russia in 2000 and in Germany in 2005, and clinical studies have been carried out in the Netherlands and Sweden (Mehmet Emin ORHAN 2008) . The use of Xe as an anesthetic creates an advantage considering the clinical effects on patients as well as ozone depletion and global warming problems (Goto 2002) .It has been discussed in the literature that the N_2O gas used in anesthesia damages the ozone layer, creates greenhouse gas effect 230 times stronger than carbon dioxide (Goto 2002). Commonly used anesthetics such as isoflurane, sevoflurane and desflurane belong to the group of hydrofluorocarbons. Their greenhouse gas-generating effects are 10 times more than carbon dioxide (Orhan 2008) . N_2O and hydrofluorocarbons are among the gases whose emissions are restricted according to the Kyoto Protocol (2008-2012), Doha Agreement (2013-2020) and Paris Agreement (2015 2030). (European policies on climate and energy towards 2020, 2030, and 2050; 2020). During the use of anesthetics, these gases spread to the atmosphere and increase the global warming problem with each day (Ljubojev, Dukić Mijatović, and Bjelajac 2017) . Otherwise, medical personnel in the operating room are also exposed to these gases emitted to the atmosphere during anesthesia. For the medical personnel who are constantly exposed to these gases; it is not known whether the gases cause carcinogenic effects. The anesthetic use of Xe therefore creates an advantage in terms of both its clinical advantage, its greenhouse gas effect or non-carcinogenic effect (Rae 2016).

1.2. **MOFs for Anesthetic Applications**

The use of nanoporous materials in separating and purifying various gas mixtures has been extensively studied in the literature (Atci & Keskin, 2012; Chen et al., 2015). Nanoporous membrane materials mainly used in the industry are zeolites (Baker, 2004; Li et al., 2011). As an alternative to zeolites and other inorganic membrane materials such as aluminophosphate, a new generation of nanoporous materials called metal organic frameworks (MOFs have been introduced in the literature, see Figure 1.2.1-a (Borboudakis et al., 2017). MOFs are high porosity organic coordination compounds that contain transition metal ions such as Zn, Cu, Co and organic linkers that bind metal atoms together. Millions of MOFs with different topologies can be synthesized by the coordination of metal ions and a wide variety of organic ligands (Borboudakis vd., 2017). The MOFs (IRMOF-1 and HKUST-1) shown in Figure 1.2.1-a are the most studied materials in the literature so

far. The network structure of Zn ion and 1,4-BDC (benzenedicarboxylate) organic ligands forms IRMOF-1 material with large pore size (10.9/14.3 Å). Cu ion and 1,3,5-BTC (benzentricarboxylate) ligands formed HKUST-1 (CuBTC) material with heterogeneous pores (3.5/5/9 Å) (Canturk, Kurt, and Gurdal 2022). Many synthesized MOFs are successfully used in gas separation processes (Adatoz, Avci, and Keskin 2015). The principle of separation of gas mixtures using MOF membranes is depicted in Figure 1.2.1-b. The gas composition fed from one surface of the membrane is different than the permeate side, since one component can diffuse faster to the other side of the membrane, depending on the physical properties of the membrane material. Similarly, in systems where MOFs are used as adsorbents, the interaction of the molecules with the MOF pores are stronger and therefore more adsorbed gas is also separated from the low-interacting gases in the mixture (Li et al. 2012).

MOFs have selective adsorption or permeation properties that enable them to be used in gas separation processes. The pore sizes of the MOFs can be designed in various sizes and the their chemical nature can be tuned by incorporating acidic or basic ligands into the framework as well as creating open metal sites in their structures., see Figure 1.2.1-c (Li et al. 2012).

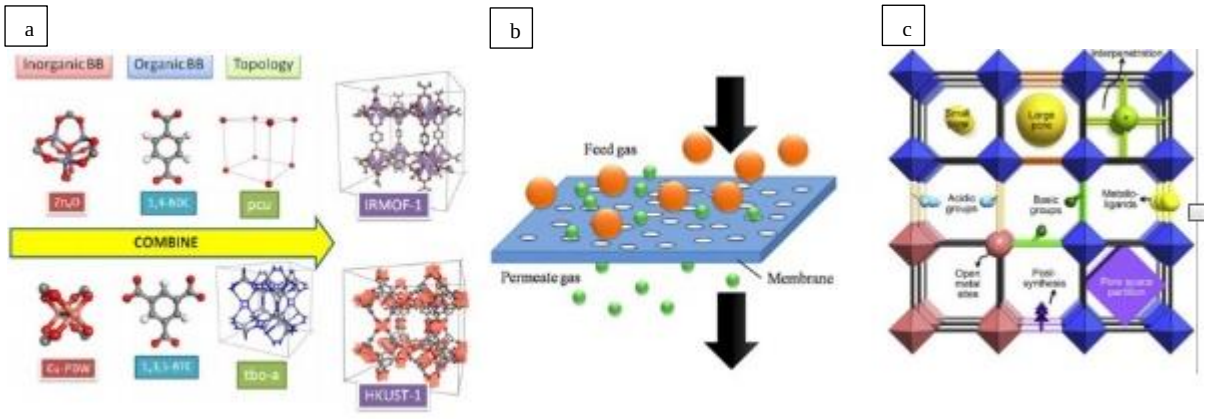

Figure 1.2.1. (a) Numerous Metal Organic Frameworks with different pore structures can be synthesized with a variety of inorganic combination building blocks suitable for many different selected framework structures. They can also be synthesized by a combination of different and very diverse organic building blocks (Borboudakis et al. 2017). **(b)** Schematic representation of separation of gas mixtures using MOF membranes (Asai et al. 2017). **(c)**

Properties of MOFs that enable them to be used in gas separation applications (Li et al. 2012).

Some portable Xe recovery devices for clinical use have been proposed, albeit slightly, in the literature, and several patents have been obtained. In the patent taken by Georgieff and Bader (1996), Xe is liquefied at high pressure (66 bar) and separated from the exhale gas mixtures using (soda-lime). In the proposed patent, although soda-lime is economically feasible, liquefying the exhale gas mixture by applying high pressure increases the energy cost (Canturk et al. 2022).

A patent proposed by Burov suggests using activated carbon and freezing the exhaled gas mixture first by decreasing temperature to -197 °C, then the system is heated and Xe is separated form the mixture by the difference of the boiling points of the exhale gas mixture components. However, this method also requires high energy and therefore high capital and operating costs (Burow 2000) which avoid the use of Xe gas recovery in the clinical industry (Burov et al. 1999).

Using MOFs for separating anesthetic Xe has been investigated using NiDOBDC, HKUST-1 and PCN-12. An adsorption-based separation of Xe at 298 K and 1 bar from the anesthetic exhaled gas mixture containing 65% Xe, 24% O_2, 6% N_2 and 5% CO_2 gases have been carried out both experimentally and theoretically. The results showed that NiDOBDC, HKUST-1 and PCN-12 had adsorption capacities of 2.62, 3.62 and 4.4 mmol/g Xe, respectively. The calculated adsorption selectivities were determined only for NiDOBDC and Xe leaves the column before CO_2 implying that Xe is less adsorbed than CO_2. Although HKUST-1 and PCN-12 show high Xe / N_2 and Xe / O_2 adsorption selectivity (approximately 18), the Xe / CO_2 adsorption selectivity was calculated as 2.3 and 1.99, respectively, for these MOFs. In this study, it was concluded that carboxylic ligands in MOF structures contribute to Xe adsorption through van der Waals interactions. However, ensuring the use of MOFs as commercial products in Xe recovery will be possible with MOFs where higher Xe / CO_2 adsorption selectivity is obtained. In addition, only the adsorption loadings have determined in this study, and membrane based separation performances of MOFs have not been investigated (Elsaidi et al. 2017).

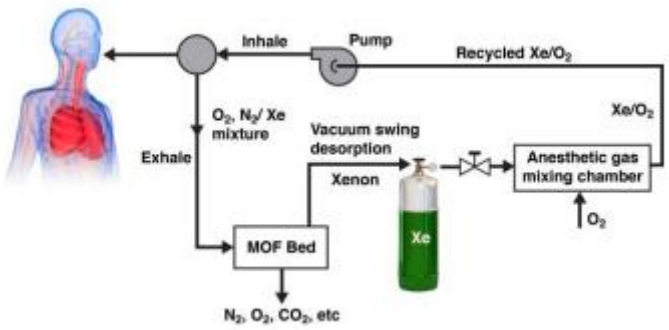

Figure 1.2.2. Schematic representation of the recovery of anesthetic Xe at room temperature using MOFs (Elsaidi et al. 2017).

In this thesis, we theoretically investigate adsorption and diffusion based anesthetic Xe separation performances of MOFs by applying Grand Canonical Monte Carlo (GCMC) and Molecular Dynamics (MD). For Xe separation, a large number of bio-MOF are screened by GCMC and MD simulations for binary mixtures of Xe, e.g. Xe/CO_2, Xe/N_2, and Xe/O_2. In this thesis, we aim to promote Xe anesthesia over conventional anesthetics in order to increase patient's recovery comfort, prevent the medical personnel from being exposed to chemicals during surgery, and to prevent the emission of the conventional anesthetic gases to the atmosphere which increase global warming effect. By investigating promising MOF adsorbents and membranes our major goal is to design a medical device that use Xe anesthesia and has a closed Xe recycling system.

2. LITERATURE REVIEW

2.1. **Metal Organic Frameworks (MOFs)**

Metal organic frameworks (MOFs) have properties such as high pore volume, low density (0.2-1 g/cm^3), high porosity, large surface area (500−6000 m^2/g). At the same time, new hybrid crystalline nanoporous materials with these beneficial physical and chemical properties have emerged. The structure-function relationship at the molecular level has the existence of multiple catalytic sites in a single MOF. On further examination, adjustable pore size, high gas uptake, good thermal and mechanical stability make them highly productive materials to be used in many studies (Chen and Jiang 2010). MOFs are observed as a highly porous structure with a wide range variation in pore size. Many different groups can be added to the structures of organic ligands. In this way, MOF pore surfaces and pore sizes can vary according to the applications. In short, it is possible to adjust the pores according to the applications. MOFs are crystalline materials. Many synthesized MOFs can retain their pore size and crystalline structure even if the solvent molecules in their structures are separated during the synthesis process (Liu et al. 2021).

When different metals are combined with organic binders, the possibilities for functions and structures change, as these combinations change the size, shape, structure and chemical affinity of the porous material. The oxidation state, coordination number, and coordination geometry are important variables in the construction of MOFs (Erucar and Keskin 2016). The coordination number of metal ions, the coordination geometry, and the nature of the functional groups affect its geometry. The chemical structural flexibility of MOFs can cause changes in the local coordination environment (Della Rocca, Liu, and Lin 2011).

MOF-5 (IRMOF-1) (isoreticular metal organic framework), one of the most studied MOFs in the literature, can be given as an example. Figure 2.1.1 shows the topology of the MOF-5. It consists of four ZnO_4 tetrahedra with a common apex and octahedral secondary structure units containing six carboxylate C atoms (Della Rocca et al. 2011).

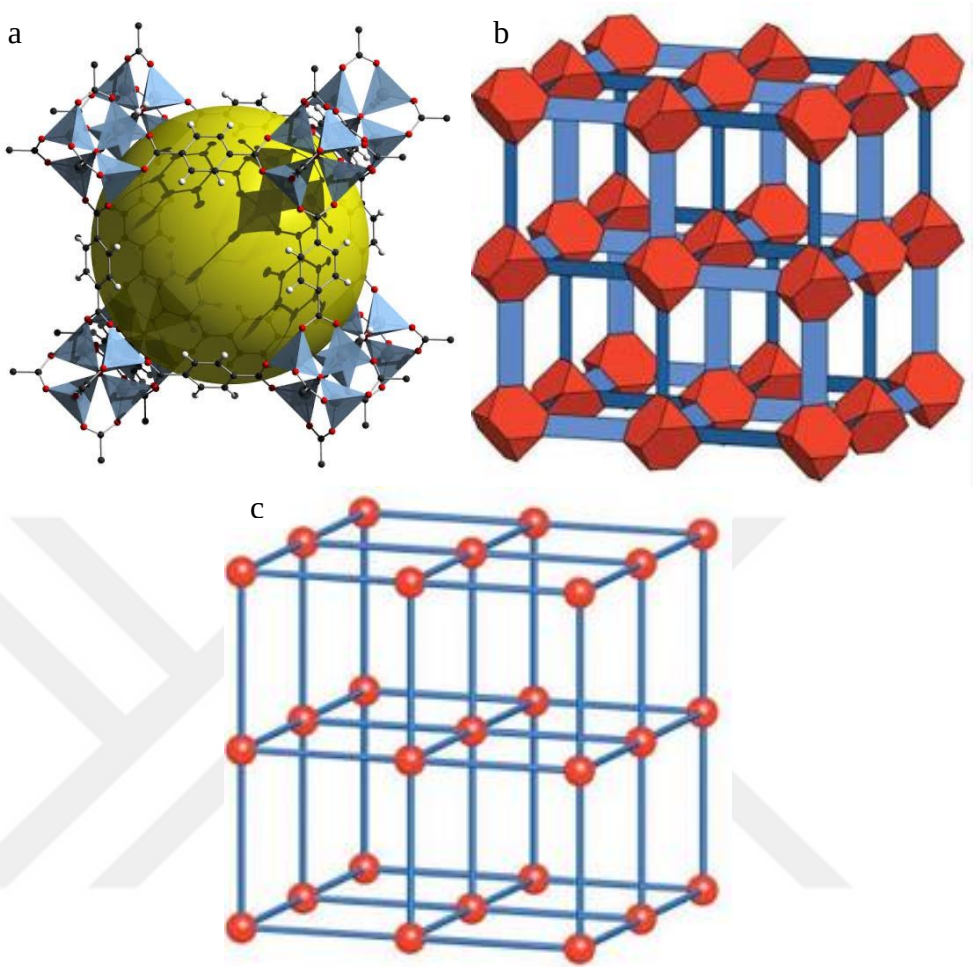

Figure 2.1.1. (a) By showing the cubic structure of MOF-5; ZnO4 tetrahedron (blue tetrahedra) combined with benzene dicarboxylate binders (OF: red and C: gray) form the MOF-5 material. ZnO4 tetrahedron (blue tetrahedra) combined with benzene dicarboxylate binders (OF: red and C: gray) form the MOF-5 material. (b) MOF-5 topologically shown as a primitive cubic shape. (c) ZnO4 shown as tetrahedron (red cut tetrahedron) and benzene dicarboxylate (blue lath).(Yaghi et al. 2003).

Figure 2.1.2 shows the potential applications of MOFs in different fields, taking into account the increase in the number of publications. As seen in Figure 2.1.2, MOF research on "adsorption" has a maximum number of publications from 1998 to 2014 with a total of 2776 articles. It is seen that a total of 762 and 953 articles were written on gas storage and separation applications of MOFs, respectively. Research on the drug storage and delivery applications of MOFs is a relatively new field compared to those years. It has a minimum total article number of 99 (Chong-Chen Wang 2016).

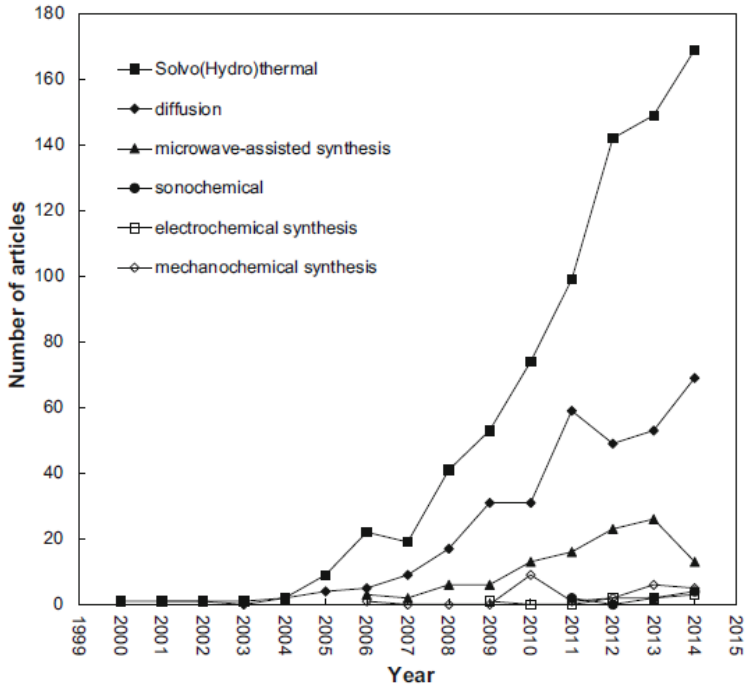

Figure 2.1.2. Number of articles on different potential applications of MOFs (Chong-Chen Wang 2016).

Binding molecules such as amino acids, nucleobases and sugars, and some biomolecules such as biocompatible metal cations have been used to form bio-MOFs (Imaz et al. 2011). Using the building blocks of biomolecules, Rosi and colleagues(An, Geib, and Rosi 2009) used adenine as ligand and zinc salts as metal centers. Bio-MOF-1 was synthesized as the first member of the bio-MOF group. Research on bio-MOFs is considered to be in its infancy. At the same time, there are only nine adenine-based bio-MOFs (1, 11, 12, 13, 14, 100, 101, 102, 103) synthesized in the literature to date (An et al. 2009).

Bio-MOFs are also used in medical fields such as drug storage or drug delivery (Ilknur Erucar 2016). They are very useful for drug loading and biodegradability. For example, one study used Bio-MOF ZnBTCA. The scientists found that this bio-MOF stores and releases a type of drug (Huang and Dan Li 2019). Because of their large pore sizes, bio-MOFs have greater storage capacities than many conventional materials. It also changes the pore size, flexibility and interconnectivity. Thus, diffusion of gas and drug molecules through the pores is controlled by modulating host interactions with organic binders and non-toxic metals of bio-MOFs. Some

biological molecular symmetries in MOFs are not suitable for synthesizing crystalline materials due to their flexible nature. However, work on bio-MOFs continues, as do work in other fields.

2.2. Separation of Xe from Anesthetic Gas Mixtures Using MOFs

Some portable Xe recovery devices for clinical use have been suggested in the literature, albeit slightly. A few patents have been obtained on the subject. Some of the studies on the recovery of anesthetic Xe in the literature are included in this study. In the patent received by Georgieff and Bader (1996) , it is proposed to liquefy Xe at high pressure (66 bar) and to separate it from the exhaled gas mixture using soda-lime (soda-lime). However, in this application, although the soda-lime material seems to be economically viable, liquefying the exhaled gas mixture by applying high pressure increases the energy cost (Gulcay and Erucar 2019).

In another study, (Burov et al. 1999), it was frozen using activated carbon and exposing the exhaled gas mixture to a temperature of -197 ^{o}C first. It is suggested that the system is then heated and separated from the exhaled gas mixture by slow boiling of Xe. However, this method also avoids the use of Xe gas recovery in the clinical industry, as it requires high energy and therefore high capital and operating costs (Elsaidi et al. 2017). based on adsorption of Xe at 298 K and 1 bar from anesthetic exhaled gas mixture containing 65% Xe, 24% O_2, 6% N_2 and 5% CO_2 using MOFs such as NiDOBDC, HKUST-1 and PCN-12. The separation has been studied both experimentally and theoretically. The results showed that NiDOBDC, HKUST-1 and PCN-12 have Xe adsorption capacities of 2.62, 3.62 and 4.4 mmol/g, respectively. The calculated adsorption selectivities were only in NiDOBDC where Xe was separated from the column before CO_2. Therefore, it has been shown that it adsorbs less than CO_2. HKUST-1 and PCN-12 showed high Xe/N_2 and Xe/O_2 adsorption selectivity. However, (about 18) Xe/CO adsorption selectivity was calculated as 2.3 and 1.99 for the mentioned MOFs, respectively. In the study, it was concluded that carboxylide ligands in MOF structures contribute to Xe adsorption by van der Waals interactions. However, the use of MOFs as commercial products in Xe recovery will be possible with MOFs that will achieve higher Xe/CO_2 adsorption selectivities.

Using DD3R zeolite membrane, it has 5%, 65% and 30% mixing ratio of Xe, respectively. He studied the separation of CO_2, Xe, and N_2 from the gas mixture both experimentally and theoretically. The CO_2 permeability at 298 K and 3 bar was measured as $2x10^{-8}$ mol m^{-2} s^{-1} Pa^{-1}. At the same time, the CO_2/Xe selectivity was found to be 67. The N_2 permeability was

measured as $2.4x10^{-9}$ mol m^{-2} s^{-1} Pa^{-1}. The N_2/Xe selectivity was calculated as 8. The results show that CO_2 and N_2 can be separated from Xe by membrane-based separation method using DD3R zeolite. However, the effect of O_2 in the exhaled anesthetic mixture on Xe recovery was not investigated in the study. In addition, no analysis on MOF structure-separation performance was performed. It has not been investigated that CO_2 and N_2 diffusion faster than Xe in the DD3R membrane (Chong-Chen Wang 2016).

3. MATERIALS AND METHODS

3.1. Selection of The Bio-MOF

The Bio-MOFs that we aim to investigate have been previously examined by (Gulcay and Erucar 2019) for O_2 separation from the O_2/N_2 mixture. They screened the Cambridge Structural Database (CSD) for the MOFs having biological linkers, surface areas larger than 0 m^2/g and pore limiting diameter (PLD) greater than 3.4 Å and found 315 structures. We further narrowed the list by eliminating the Bio-MOFs having linkers which may be toxic during synthesis and use, such as cyanamide, phthalate, carbazole. Bio-MOFs containing lanthanide group elements such as Pr, In, La, Er, Tm, Yb, Dy, Ho, Y, Lu, Gd, Ce Tb, Eu, Sm are also excluded from the list, since they are rare in nature. In addition, Bio-MOFs containing metals such as Cr, Cd and Cs, which may create toxic properties, and bio-MOFs containing Ru, Rh and Rb in their structures are also excluded from the list in order to reduce the cost during synthesis. Furthermore, pore limiting diameter (PLD), surface area, and void fraction are also applied as additional criterias for selecting the Bio-MOFs. From the remaining list, we study the Bio-MOFs having PLD, void fraction, and surface area larger than 4.5 Å, 0.25, and 500 m^2/g, respectively. As a summary, we investigate in total 43 Bio-MOFs, see Appendix, that have adenine, amino, formadide, formate, porphyrin, muconate, and tricarboxylate linkers in their structures. In terms of metal diversity, the Bio-MOFs under consideration have Zn, Cu, Co, Ni, Mn, Mg, Na, and Zr elements in their structures. The atomic positions of the selected Bio-MOFs are taken from the Computation-Ready, Experimental Metal Organic Framework Database (CoREMOF Database) (Randall Q. Snurr 2019).

Geometric representations of some of these MOFs are shown in Figure 3.1.1. These geometric representations are taken from the Mercury visualization tool (Macrae et al. 2020). Rigid structures of MOFs are used in our simulations:

ADASOP

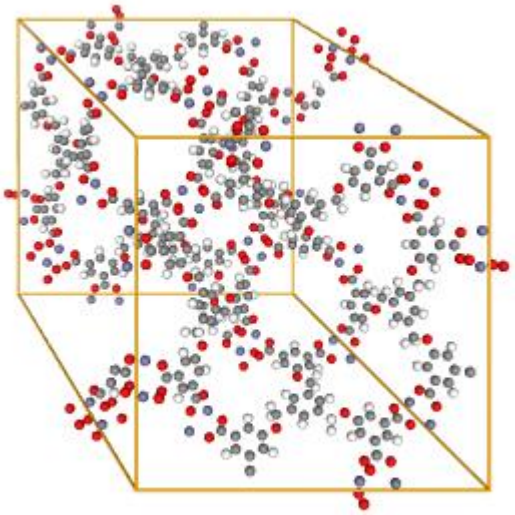

BEDYEQ

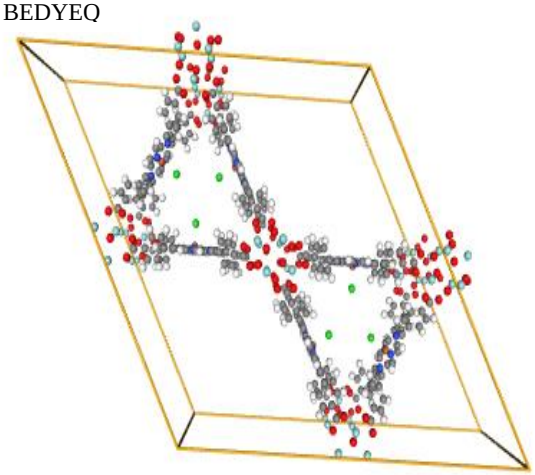

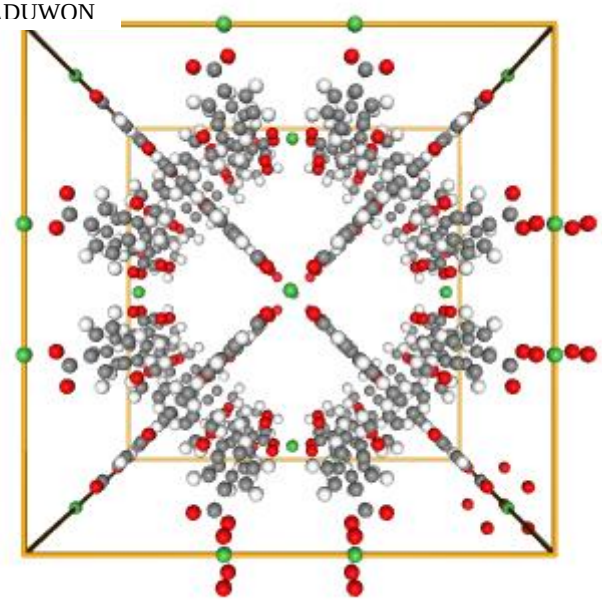

Figure 3.1.1. Bio-MOFs under Consideration in Mercury.

3.2. Grand Canonical Monte Carlo (GCMC) Simulations for Adsorption

Binary gas adsorption isotherms and gas dffusivities of Xe/CO_2, Xe/O_2, and Xe/N_2 mixtures are calculated using the Grand Canonical Monte Carlo (GCMC) and molecular dynamics simulations, respectively. GCMC and MD simulations are carried out using the open source RASPA package which has been applied successfully for determining gas adsorptions and permeations inside nanoporous material (Lagorsse, Magalhães, and Mendes 2007) .

Interactions between the adsorbate-adsorbate and adsorbate-adsorbent are modeled using the Lennard-Jones (LJ) potential , electrostatic interactions are described using the Coulomb potential, thus the formulation for the binary interaction potential between atomic species is calculated (Verlet 1967).

Atomic force field paramters of the Bio-MOF atoms for calculating dispersion interactions are obtained from Universal Force Field (UFF). The UFF force field have been widely used in the literature and theoretical results have been successfully compared with the experimental ones (Gurdal and Keskin 2012). The dispersion interaction force field parameters between different kinds of atoms are calculated using the Lorentz Berthelot mixing rules (Chen, Mi, and Chan 2001). While electrostatic interactions are also taken into account for CO_2, O_2, and N_2 molecules, Xe is considered to be

interacting only through dispersion type of interactions with the adsorbent as well as adsorbates. The LJ force field parameters for the Xe atom are taken from previous modeling studies (Daglar and Keskin 2018). The CO_2 molecule is modeled as a 3-site linear and rigid molecule and point atomic charges are placed at the center of each site to account for the first-order electrostatic and second-order induction interactions (Perez-Carbajo et al. 2018). The bond lengths, C-O, and bond angle, O-C-O, are xed at 1.149 Å and 180^o, respectively. While CO_2 is modeled as a 3-site model and each site corresponds to an atom center, for modeling N_2 and O_2 central dummy pseudo-atoms (DN and DO) having non-zero charges and zero LJ parameters and mass are de_ned to approximate electrostatic moments of N_2 and O_2. The N atoms are separated by 1.10 Å whereas O_2 bond length is set to 1.208 Å. The force field parameters of the components used in simulations are summarized in Appendix.

Electron density distributions are computed at the Kohn-Sham Density Functional Theory (DFT) level employing the Gaussian and plane wave (GPW) formalism as implemented in the CP2K package (Manz 2017). The general gradient approximation (GGA) by Perdew Burke Enzerhof (PBE) is used as density functional and dispersion interactions are included using Grimme-D3 scheme (Grimme et al. 2010; Perdew, Burke, and Ernzerhof 1996). While valence electrons are treated explicitly, norm-conserving Goedecker Teter Hutter (GTH) pseudo potentials are used to compute the interactions between the valence electrons and the atomic cores. Double-zeta valence plus polarization (DZVP) basis sets, optimized on molecular geometries (Mol-Opt method) , are employed for all atomic kinds (Goedecker, Teter, and Hutter 1996; VandeVondele and Hutter 2007). A cut off 500 R_y is used for the auxiliary plane wave basis set. Periodic boundary conditions and spin polarization are always applied.

Table 3.2.1 Force field parameters and atomic point charges used for the adsorbates are reported. D_O and D_N stand for central dummy pseudo-atoms assigned to O_2 and N_2, respectively.

Component	ε/k_B(K)	σ (Å)	q (e^-)
Xe	221.0	4.1	-
C_{CO_2}	29.933	2.745	0.652
O_{CO_2}	85.671	3.017	-0.326
O_{CO_2}	48.158	3.033	0.112
D_{CO_2}	-	-	0.224
N_{CO_2}	38.298	3.306	-0.405
D_{CO_2}	-	-	0.801

3.3. Molecular Dynamics (MD) Simulations

Molecular dynamics (MD) simulation is a computational simulation technique that used to understand the behavior of nano-suspensions and nanocomposites containing nanoparticles of various shapes and chemical functionality at both atomic and molecular levels. The MD simulation technique is based on using Newton's equations of motion to determine the positions of particles in classical theory. Interatomic potential functions and molecular mechanical force fields are used to define the forces that exist between particles (Meenakshi Dutt 2011).

If any thermodynamic propelling force that can induce fluxes in the system is removed, Molecular Dynamics (MD) is utilized to calculate the balance and bearing properties of a traditional many-body system. An N-particle system is used to select intramolecular dynamics. The initial locations and speeds are assigned (initialization). Each particle's forces are calculated. Actual measurements are taken after equilibration, and this stage is referred to as production. When the ensemble average equals the temporal average of any function A, as demonstrated below, ergodicity plays a critical role (Seda Keskin 2011)

Ensemble averaged structural and thermodynamic properties from an equilibrated MD simulation can be computed using the ergodicity assumption. The dynamics of a single system are followed by a molecular dynamics simulation, which generates averages of the form. The following potential energy formula should be used when determining forces on each particle:

$$U = \sum_{i}^{N} u_1(r_i) + \sum_{i}^{N}\sum_{j>i}^{N} u_2(r_i, r_j) + \sum_{i}^{N}\sum_{j>i}^{N}\sum_{K>J>i}^{N} u_3(r_i, r_j, r_k) + \cdots (1)$$

The effects of the external field on the system are represented by the first term in Equation 1. Higher order particle interactions are described by other termsPeriodic boundary conditions (PBCs) are a type of boundary condition that generally applied in Molecular Dynamics to prevent problems with boundary effects caused by finite size and to make the system more infinite system, at the expense of possible periodicity effects (Sumit Sharma 2019) . Figure 3.3.1 schematically illustrates the concept of the periodic boundary condition for a two-dimensional system. Periodic boundary conditions can be used to create a system that is bounded but free of physical walls. The center simulation box is replicated throughout space to accomplish this. One of a molecule's images enters from the opposite side when it leaves the central box from one side. Short-range interactions, such as dispersive and repulsive effects, are eliminated, and long-range electrostatic interactions can be handled via Ewald summation. Molecules might be rigid, flexible, or a combination of the two. The majority of computation time in most MD simulations is spent on computer interactions, and every effort is taken to make this as efficient as possible. Interactions can be determined using a simple table lookup, possibly with interpolation for enhanced accuracy, as an alternative to direct evaluation (Chen and Jiang 2010).

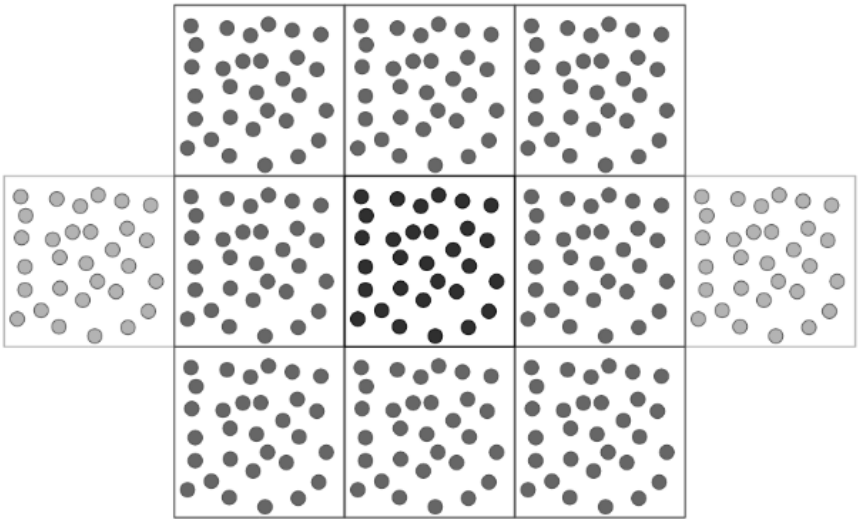

Figure 3.3.1. Periodic Boundary Conditions (Sumit Sharma 2019).

3.4. Evaluation of the Bio-MOF Performance Metrics

Adsorption based separation performance metrics of the Bio-MOFs under consideration are determined by calculating Xe adsorption selectivity of the materials for Xe/CO_2, Xe/O_2, and Xe/N_2 mixtures, as depicted below:

$$S_{ads\left(\frac{i}{j}\right)} = \frac{{c_i}/{c_j}}{{y_i}/{y_j}} (2)$$

where c and y are the molar fractions of the adsorbed and bulk phases, respectively. While c values are determined by GCMC simulations, the gas composition of the Xe in all of its binary gas mixtures is set to 80%, thus y_{Xe} is set to 0.8 and the y_{CO2} (y_{O2} or y_{N2}) is set to 0.2.

We further characterize adsorption based Xe separation performances of the Bio-MOFs under consideration by calculating their absolute gravimetric (Ng, wt.%) and volumetric (Nv, g/L) Xe uptakes, as depicted below:

$$N_g(wt.\%) = \frac{c_{Xe} m_{Xe}}{M_{MOF} + c_{Xe} m_{Xe}} \times 100 (3)$$

$$N_v = \frac{c_{Xe} m_{Xe}}{V_{MOF}} \quad (4)$$

where c_{Xe} is the total number of Xe adsorbed in a unit cell, m_{Xe} is the atomic mass of Xe, M_{MOF} is the atomic mass of the unitcell and V_{MOF} is the volume of the unit cell.

Membrane based separation performances of the Bio-MOFs are evaluated by calculating Xe permeability and Xe permeation selectivity for all binary gas mixtures of Xe at 5 bar pressure and 298 K, as shown below:

$$P_i = \frac{D_{self,ic_i\varphi}}{f_i} \quad (5)$$

$$S_{ij} = \frac{D_{self,i} c_i}{D_{self,i} c_i} \frac{f_i}{f_i} \quad (6)$$

where c_i and c_j are adsorbed loadings of species i and j in *i=j* mixture calculated using GCMC simulations, ϕ is fractional porosity of the Bio-MOFs, and f_i (f_j) is fugacity of the specie *i (j).*

4. RESULTS AND DISCUSSIONS

We first compare the adsorption loadings of the Bio-MOFs under consideration for each gas mixtures, Xe/CO_2, Xe/O_2, and Xe/N_2. The Xe molar composition is always set to 80% in these mixtures where the rest is supplied by the other component, e.g. CO_2, O_2, or N_2 Figure 4.1. shows the adsorption loadings of the gas components, where y axis shows the Xe adsorption and x axis depicts the CO_2, O_2, or N_2 loadings in molecules/unitcell. We plot all adsorption values of each gas component calculated for a pressure range from 0.1 bar to 10 bar, 14 pressure points in total. Thus, considering 43 Bio-MOFs in total, in each figure we plot 602 data points. The comparison of Xe and CO_2 loadings for Xe/CO_2 mixture is plotted in Figure 4.1-(a). As a general observation, at low pressures Xe and CO_2 loadings of the Bio-MOFs are comparable with each other, however as pressure increases, we see sharp increase in the Xe adsorption capacity for some of the Bio-MOFs. Among the 43 Bio-MOFs under consideration, ZEZFIV, AGOFEJ, BEDYEQ, BIPSUQ, BEWCUD, ADASOP, and ADUWON are the materials that show signiffcantly large Xe uptake over CO_2 especially at pressures between 3 to 10 bar. At 5 bar, Xe and CO2 loadings of the BIPSUQ (BEWCUD) are calculated as 65 (70) and 10 (15) molecules/unitcell and as pressure increases to 10 bar loadings of the Xe and CO_2 increase to 117 (112) and 21 (29), respectively. Although, mentioned 6 Bio-MOFs show exceptionally high tendency for Xe adsorption, there are a few Bio-MOFs which favor CO_2 adsorption over Xe. For instance, at 10 bar CO_2 adsorption of LONWIW, EZOFEF, and WURKEB are calculated as 26, 11, and 15 molecules/unitcell, respectively. For Xe, on the other hand, the adsorption capacities of these MOFs are determined as 9, 11, and 15 molecules/unitcell, respectively.

For the Xe/O_2 mixture, we observe a similar adsorption trend as we obtain for the Xe/CO_2 mixture. The aforementioned seven Bio-MOFs show large Xe uptake over O_2 for higher pressure range of 3 to 10 bar, as depicted in Figure 4.1-(b). As in the case of Xe/CO_2 mixture, BIPSUQ and BEWCUD show the largest Xe uptake at 10 bar feed pressure. Apart from them, at 5 bar Xe and O_2 loadings of the ADASOP (ADUWON) are calculated as 64 (73) and 16 (15) molecules/unitcell and as pressure increases to 10 bar loadings of the Xe and O_2 increase to 79 (91) and 27 (25), respectively. EZOFEF and XACZEH, on the other hand, show comparable O_2 uptake with respect to Xe. For the Xe/N_2 mixture, we see signicantly larger Xe loading with respect to N_2 for all the Bio-MOFs under considerarion. The same set of Bio-MOFs again shows the largest Xe uptake for the Xe/N_2 mixture.

Xe adsorption selectivities calculated for three mixtures are depicted in Figure 4.2. Promising adsorbents should show both larger uptake as well larger adsorption selectivity for the desired specie separated from its mixture by adsorption. According to Figure 4.2-(a), BEYSEF, BEPMAM, CETHEQ, FIQCEN, and IZUMUM show larger Xe selectivities for the Xe/CO2 mixture, however, their Xe loadings are significantly lower. Previously mentioned 6 Bio-MOFs, on the other hand, possess Xe adsorption selectivity around 1 for feed pressures from 5 to 10 bar. At lower pressures, on the other than, these Bio-MOFs show relatively larger Xe selectivity between 1.2 to 2. The same behavior is also obtained for the Xe/O_2 mixture, where 6 Bio-MOFs showing larger Xe uptake possess Xe adsorption selectivity between 1.2 and 2.2, and as pressure increases these materials adsorb Xe and O_2 with the same selectivity. Some materials, such as ADAXIO and LUSHOX, on the other hand, show higher Xe adsorption selectivity, around 5, at low pressures. However, as pressure increases, Xe selectivity decreases sharply and some materials even become O_2 selective, e.g. DUBWON, FIQCEN. All materials under consideration show signi_cantly large Xe adsorption selectivity for the Xe/N_2 mixture. ADAXIO, DOMKEX, LIXWAR, and LUSHOX show Xe adsorption selectivity ranging between 60 and 90 at low pressures. The 6 Bio-MOFs that show the largest Xe uptake with respect to CO_2 or O_2 species show large Xe selectivity (around 10) for the Xe/N_2 mixture at considered pressure range.

In addition to adsorption loadings and selectivity, volumetric and gravimetric adsorption loadings of the nanoporous materials are also key factors for determining the efficiency of the adsorbents with respect to each other for scale-up purposes. Figure 4.3. compares the gravimetric (wt%) and volumetric (g/L) Xe adsorption loadings of 43 Bio-MOFs for the three binary mixtures of Xe at the same set of feed pressure range, 0.1 to 10 bar.

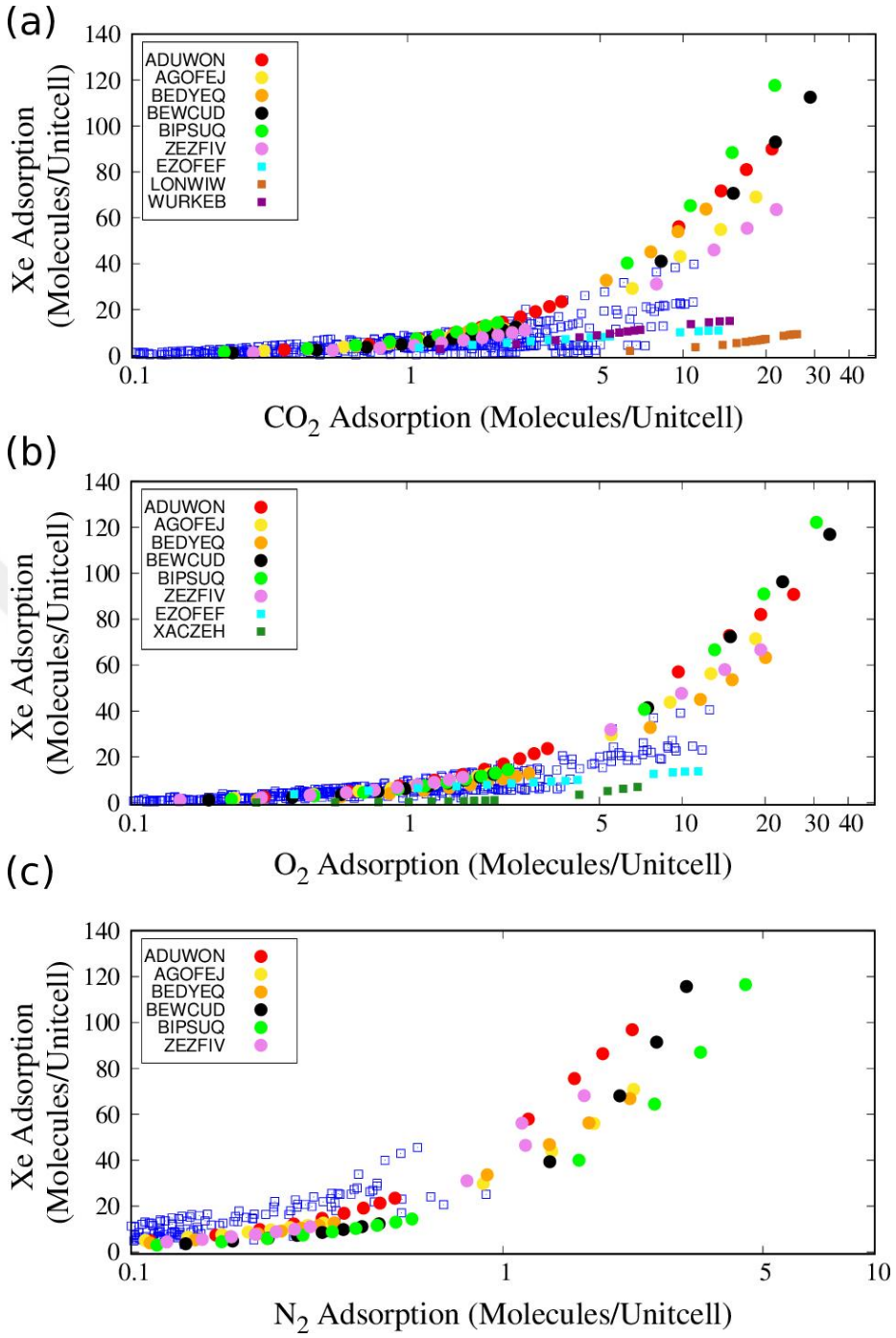

Figure 4.1. Adsorption loadings of (a) Xe and CO_2 in Xe/CO_2:80/20 mixture, (b) Xe and O_2 in Xe/O_2:80/20 mixture, and (c) Xe and N_2 in Xe/N_2:80/20 mixture. Closed circles are used to depict the 6 Bio-MOFs having larger Xe adsorption loadings with increasing pressure, open blue squares are used for the rest of the Bio-MOFs. Closed squares represent the materials having larger CO_2 or O_2 uptake with respect to Xe.

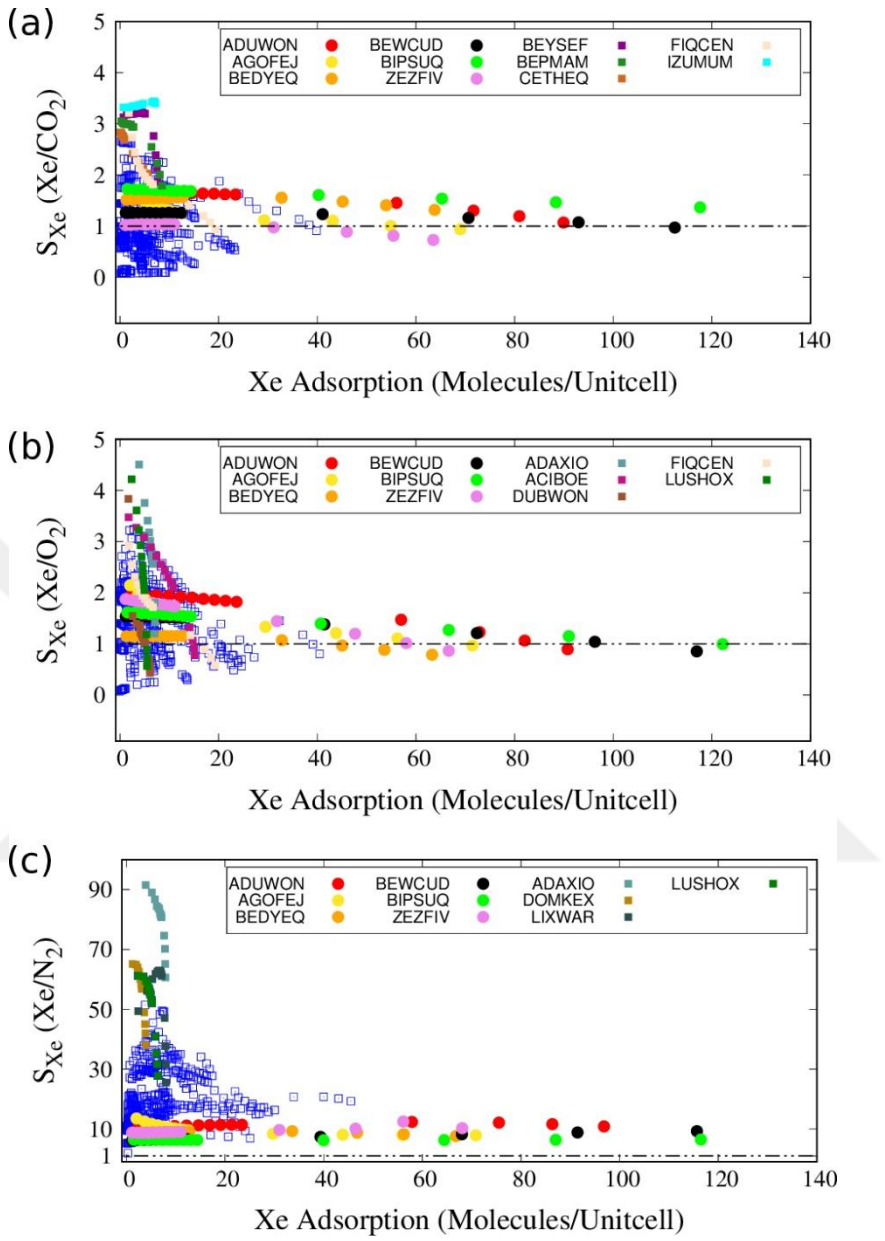

Figure 4.2. Xe adsorption selectivities, S_{Xe}, calculated for (a) Xe/CO_2:80/20 mixture, (b) Xe/O_2:80/20 mixture, and (c) Xe/N_2:80/20 mixture. Closed circles are used to depict the 6 Bio-MOFs having larger Xe adsorption loadings with increasing pressure, open blue squares are used for the rest of the Bio-MOFs. Closed squares represent the materials having larger Xe selectivity but lower Xe uptake.

As pressure increases, we observe sharp increase for both volumetric and gravimetric Xe a sorptions for the 6 Bio-MOFs for all binary mixtures of Xe. For instance, at 10 bar feed pressure, gravimetric and volumetric Xe adsorptions of the BEWCUD are calculated around 60 wt% and 1000 g/L, respectively. These results suggest that the 6 Bio-MOFs are, indeed, promising candidates for separating Xe from it binary mixtures with CO_2, O_2, or N_2. Structural information of the Bio-MOFs under consideration gives hint on the preferable adsorption of Xe over CO_2, O_2, or N_2 observed especially for the 6 Bio-MOFs. Figure 4.3-(a) and (b) depict pore sizes and void fraction versus surface area information of the Bio-MOFs under consideration. The largest cavity diameter (LCD) and pore limiting diameters (PLD) of the Bio-MOFs range from 5-32 Å for LCD and 4.5-31 Å for PLD. The 6 Bio-MOFs showing the largest Xe uptake with respect to the other gas components, have PLD and LCD larger than 5.5 and 10 Å, respectively. The one another common feature of these Bio-MOFs is that they possess larger void fraction as well as surface area with respect to the other Bio-MOFs under consideration. While void fraction of the Bio-MOFs are around 0.8, they exhibit surface areas larger than 2900 m^2/g. These results suggest that for separating anesthetic Xe, one could seek for materials having large pore sizes, large void fractions, as well as large surface areas. The adsorption strength is characterised by heat of adsorption values which are provided in Figure 4.4-(c), (d), and (e) for the Xe/CO_2, Xe/O_2, and Xe/N_2 mixtures, respectively. As a general observation, Bio-MOFs having larger pore sizes, void fractions, and surface areas possess lower heat of adsorption for Xe which is an expected result, due to the lower connement of Xe in the larger pores. The comparison of heat of adsorption for Xe, CO_2, and O_2 reveal that the components feel the similar adsorption strenght in the pores of the materials. In the case of Xe/N_2, on the other hand, due to the lower energy parameter of N_2, heat of adsorption for Xe is always larger than the ones calculated for the N_2.

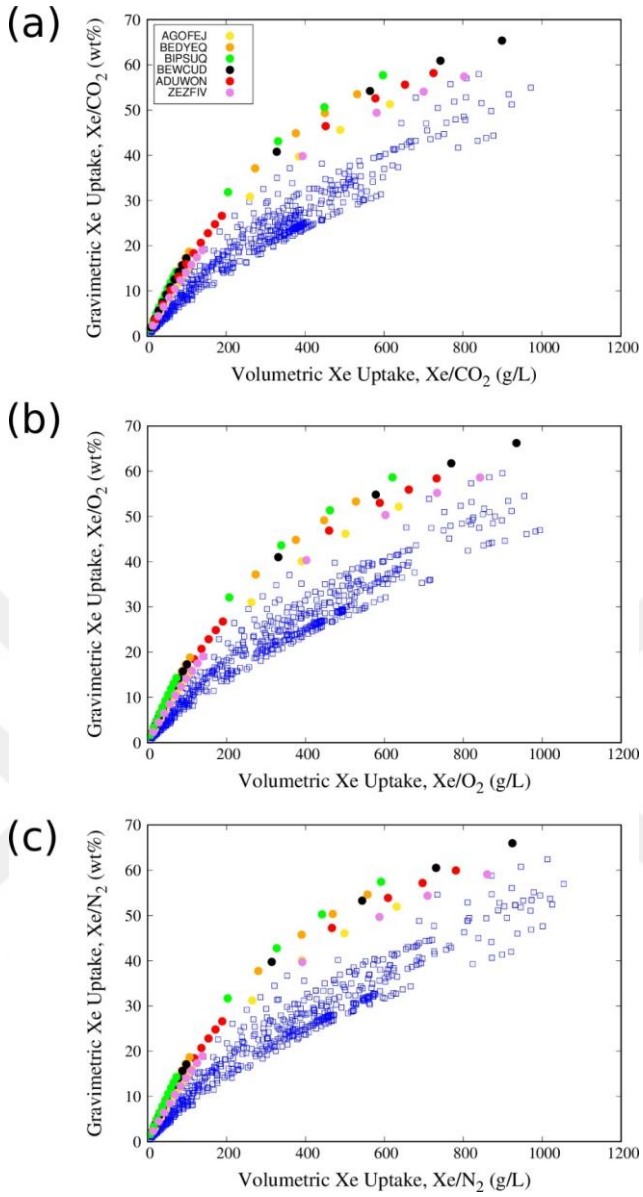

Figure 4.3. Gravimetric (wt%) versus volumetric (g/L) Xenon adsorption of the Bio-MOFs for (a)Xe/CO_2:80/20, (b) Xe/O_2:80/20, and (c) Xe/N_2:80/20 mixtures. Closed circles are used to depict the 6 Bio-MOFs having larger Xe adsorption loadings with increasing pressure, open blue squares are used for the rest of the Bio-MOFs.

Structural information of the Bio-MOFs under consideration gives hints on the preferable adsorption of Xe over CO_2, O_2, or N_2 observed especially for the 6 Bio-MOFs. Figure 4.4-(a) and (b) depict pore sizes and void fraction versus surface area information of the Bio-MOFs under consideration. The largest cavity diameter (LCD) and pore limiting diameters (PLD)

of the Bio-MOFs range from 5-32Å for LCD and 4.5-31Å for PLD. The 6 Bio-MOFs showing the largest Xe uptake with respect to the other gas components, have PLD and LCD larger than 5.5 and 10 Å, respectively. The one another common feature of these Bio-MOFs is that they possess larger void fraction as well as surface area with respect to the other Bio-MOFs under consideration. While void fraction of the 6 Bio-MOFs is around 0.8, they exhibit surface areas larger than 2900 m^2/g. These results suggest that for separating anesthetic Xe, one could seek materials having relatively large pore sizes, large void fractions, as well as large surface areas. The adsorption strength is characterised by heat of adsorption values which are provided in Figure 4.4-(c), (d), and (e) for the Xe/CO_2, Xe/O_2, and Xe/N_2 mixtures, respectively. As a general observation, we obtain relatively high heat of Xe adsorption for all the Bio-MOFs under consideration. However, Bio-MOFs having larger pore sizes, void fractions, and surface areas possess lower heat of adsorption for Xe. For the Bio-MOFs having narrower pores, on the other hand, we observe stronger connement of guest molecules which leads to larger values of heat of adsorption.

The comparison of heat of adsorption for Xe, CO_2, and O_2 reveal that the components feel similar adsorption strength in the pores of the materials. In the case of Xe/N_2, on the other hand, due to the lower energy parameter of N_2, heat of adsorption for Xe is always larger than the ones calculated for the N_2. The calculated heat of adsorption values are comparable to the experimental studies.

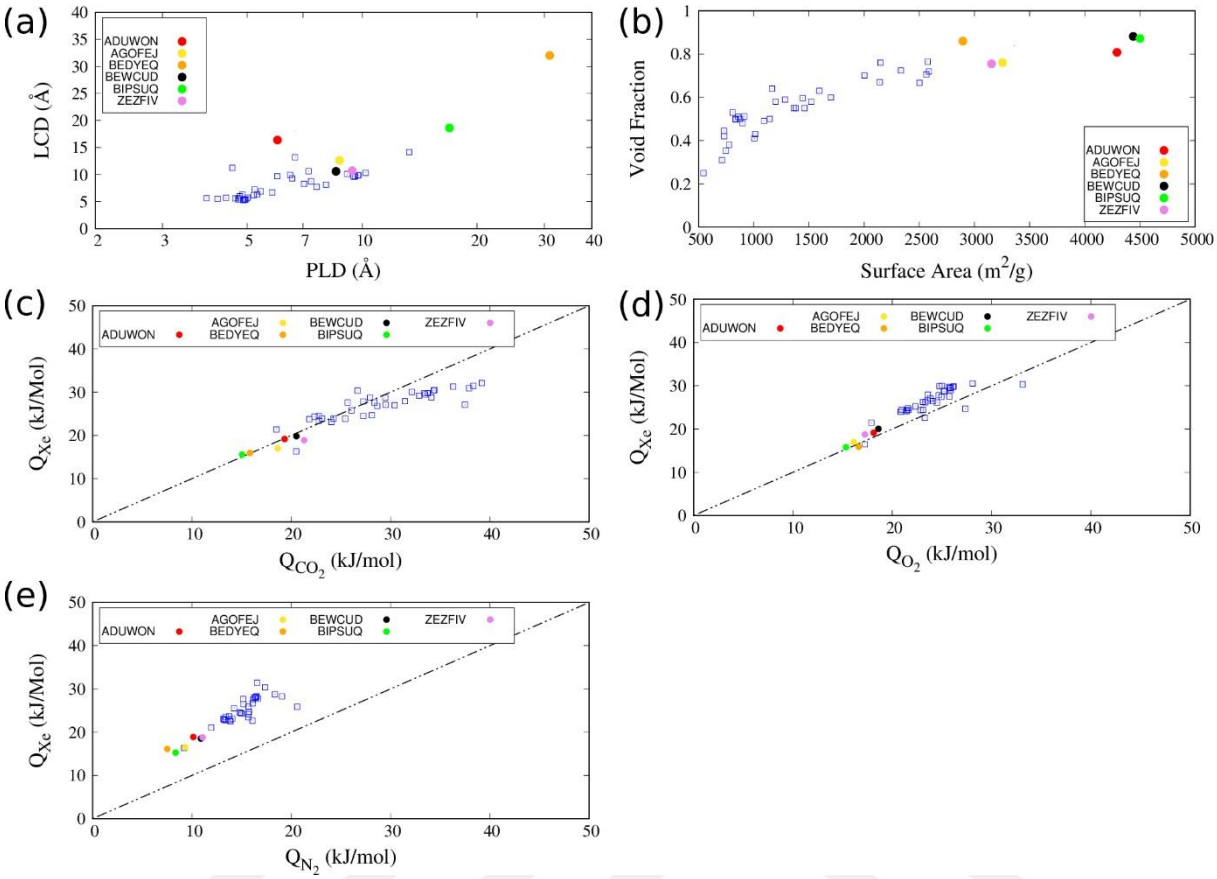

Figure 4.4. Structural information of the Bio-MOFs are given in terms of (a) the largest cavity diameter (LCD) versus the pore limiting diameter (PLD) and (b) void fraction versus surface area (m^2/g). Heat of adsorption (kJ/mol) calculated at 10 bar and 298 K for the species in the (c) Xe/CO_2, (d) Xe/O_2, and (e) Xe/N_2 mixtures are provided.

4.1. Comparison of Charge calculation Methods

Two different methods, both EQeq Method and DDEC6 method, were compared. In the DDEC6 calculation, exactly one electron was assigned to each atom. It has been determined that the DDEC6 method is a more accurate charge calculation method than the EQeq method, since the electrons are assigned to the correct host atom.

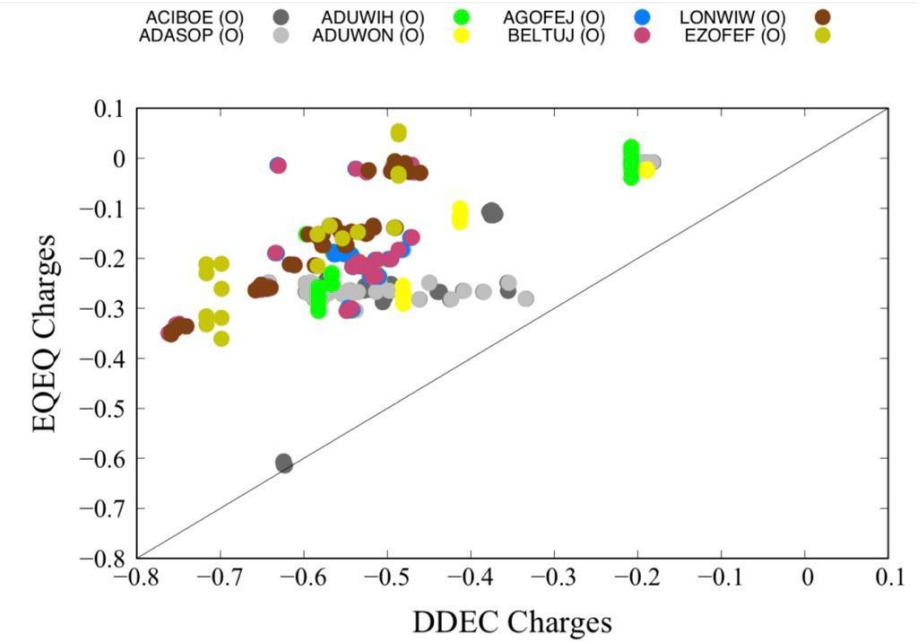

Figure 4.1.1. Charges of O atoms computed by DDEC and EQeq.

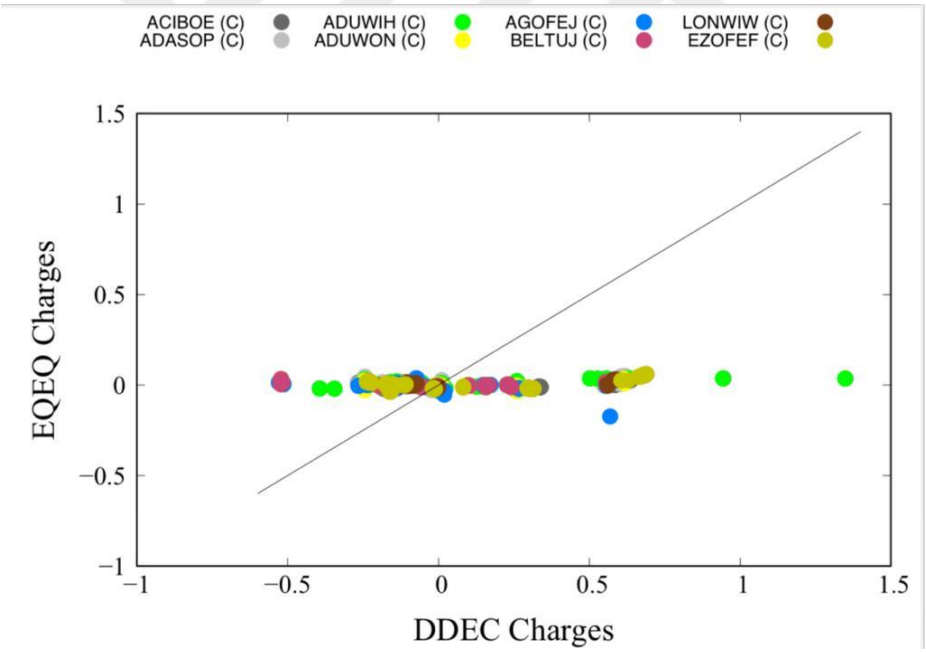

Figure 4.1.2. Charges of C atoms computed by DDEC and EQeq.

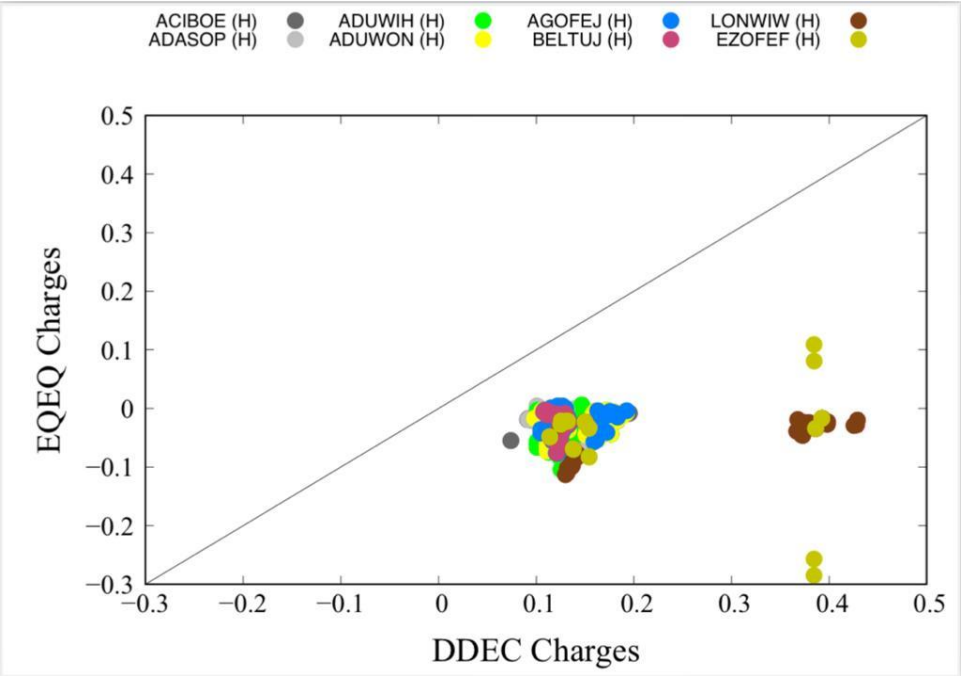

Figure 4.1.3. Charges of H atoms computed by DDEC and EQeq.

4.2. Molecular Dynamics Investigation for Membrane-based Performances

Mixture MD simulations are carried out to determine the relative dffusivities as well as permeabilities of Xe with respect to CO_2 or O_2. The selected Bio-MOFs does not much interact with N_2 molecules compared to Xe, CO_2, or O_2, thus with following calculations have been carried by omitting Xe/N_2 mixture. MD simulations are carried out at 298 K and 5 bar. Figure 4.2.1. shows the comparison of self-diffusitivies and permeabilities calculated at 5 bar for the selected Bio-MOFs. Self diffusivities for Xe for its binary mixtures with CO_2 or O_2 resemble to each other and they are generally lower than the self diffusivities calculated for the CO_2 or O_2. The 6 Bio-MOFs show very large Xe self dffusivities compared to the other materials under consideration which is attributed to their larger pore sizes and void fractions. The self dffusivity of Xe and CO_2 calculated for these 6 Bio-MOFs are larger than the experimentally determined self diffusivities in DDR3 zeolite. Xe permeabilities are also calculated larger for these 6 Bio-MOFs with respect to the rest of the materials under consideration. MD calculations suggest that Bio-MOFs with pore sizes larger than 10 Å as well as having large surface areas and void fractions could be promising candidates for separating anesthetic Xe from its binary mixtures with CO_2, O_2, or N_2.

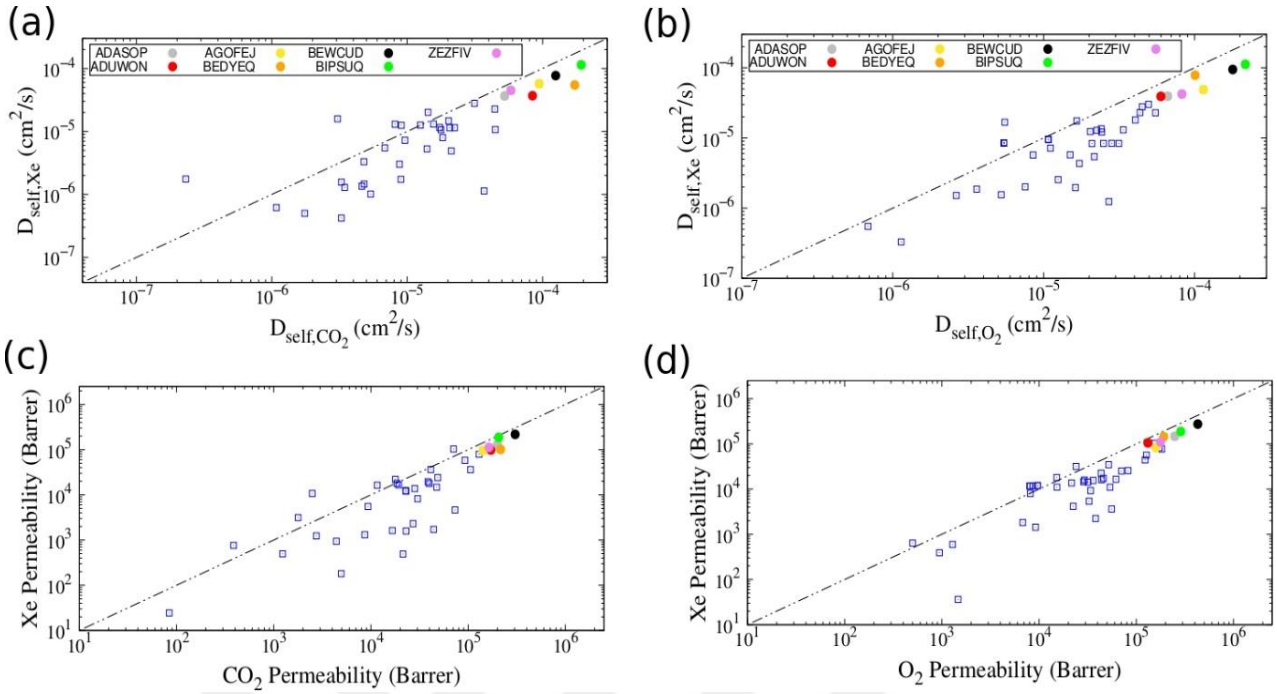

Figure 4.2.1. Self diffusivities calculated for (a) Xe /CO_2 and for (b) Xe /O_2 for and Xe/N_2.

5. CONCLUSIONS

In this work, adsorption and membrane based anesthetic Xe recovery performances of 43 Bio-MOFs are investigated by applying GCMC and MD methods. From the systematic theoretical studies, the following results are obtained:

(1) Among the 43 Bio-MOFs under consideration, ZEZFIV, AGOFEJ, BEDYEQ, BIPSUQ, BEWCUD, and ADUWON are determined as top performing materials that show significantly large Xe uptake over CO_2, O_2, and N_2 especially at pressures between 3 and 10 bar. These materials also maximize Xe adsorption both volumetrically and gravimetrically.

(2) Top performing Bio-MOFs show larger Xe adsorption selectivities over CO_2 and O_2 which are calculated between 1.2 and 2 at low pressures. As pressure increases to 5 or 10 bar, Xe adsorption selectivities decrease to 1 for these Bio-MOFs. For the Xe/N_2 mixture, on the other hand, Xe is always significantly adsorbed than N_2 for all the pressure range considered in this work.

(3) Having metalloporphyrin, hexacarboxylate, triazine, or pyrazole ligands, transition metal included paddlewheel units, relatively large pore sizes (PLD>5 Å and LCD>10 Å), large void fractions (0.8), and large surface areas (>2900 m^2/g) maximizes the Xe-pore interactions and ultimately Xe recovery performances of these top performing Bio-MOFs.

(4) The top performing Bio-MOFs show larger Xe self dffusivities as well as larger Xe permeabilities with respect to the rest of the materials under consideration.

Noncovalent chemistry of noble gases has been rarely studied in the literature. By selecting the Bio-MOFs having proper chemical and topological features, important Xe-host interactions, indeed, can be facilitated which opens the door for practical application of Xenon as an anesthetic gas.

REFERENCES

Adatoz, Elda, Ahmet K. Avci, and Seda Keskin. 2015. 'Opportunities and Challenges of MOF-Based Membranes in Gas Separations'. *Separation and Purification Technology* 152:207–37. doi: 10.1016/j.seppur.2015.08.020.

An, Jihyun, Steven J. Geib, and Nathaniel L. Rosi. 2009. 'Cation-Triggered Drug Release from a Porous Zinc-Adeninate Metal-Organic Framework'. *Journal of the American Chemical Society* 131(24):8376–77. doi: 10.1021/ja902972w.

Asai, Tomohiro, Dumitru Cebrucean, Quan Zhuang, Goncalo Carrera, Jom Wlls, Dongqi Wen, Wonjun Cho, Rouzbeh Moghanloo, John Bergstrom, and Yongseung Yun. 2017. *Recent Advances in Carbon Capture and Storage*.

Banerjee, Debasis, Cory M. Simon, Sameh K. Elsaidi, Maciej Haranczyk, and Praveen K. Thallapally. 2018. 'Xenon Gas Separation and Storage Using Metal-Organic Frameworks'. *Chem* 4(3):466–94. doi: 10.1016/j.chempr.2017.12.025.

Borboudakis, Giorgos, Taxiarchis Stergiannakos, Maria Frysali, Emmanuel Klontzas, Ioannis Tsamardinos, and George E. Froudakis. 2017. 'Chemically Intuited, Large-Scale Screening of MOFs by Machine Learning Techniques'. *Npj Computational Materials* 3(1):1–7. doi: 10.1038/s41524-017-0045-8.

Burov, N. E., L. Iu Kornienko, G. N. Makeev, and V. N. Potapov. 1999. '[Clinical and experimental study of xenon anesthesia]'. *Anesteziologiia I Reanimatologiia* (6):56–60.

Burow, Paul D. 2000. 'Lawn Waste Disposal'.

Canturk, Behra, Ali Kurt, and Yeliz Gurdal. 2022. 'Models Used for Permeability Predictions of Nanoporous Materials Revisited for H2/CH4 and H2/CO2 Mixtures'. *Separation and Purification Technology* 121463. doi: 10.1016/j.seppur.2022.121463.

Chen, J., J. G. Mi, and K. Y. Chan. 2001. 'Comparison of Different Mixing Rules for Prediction of Density and Residual Internal Energy of Binary and Ternary Lennard-Jones Mixtures'. doi: 10.1016/S0378-3812(00)00478-7.

Chen, Yifei, and Jianwen Jiang. 2010. 'A Bio-Metal-Organic Framework for Highly Selective CO(2) Capture: A Molecular Simulation Study'. *ChemSusChem* 3(8):982–88. doi: 10.1002/cssc.201000080.

Chong-Chen Wang, Yuh-Shan Ho. 2016. 'Research Trend of Metal–Organic Frameworks: A Bibliometric Analysis | SpringerLink'. Retrieved 14 July 2022 (https://link.springer.com/article/10.1007/s11192-016-1986-2).

Daglar, Hilal, and Seda Keskin. 2018. 'Computational Screening of Metal-Organic Frameworks for Membrane-Based CO2/N2/H2O Separations: Best Materials for Flue Gas Separation'. *The Journal of Physical Chemistry. C, Nanomaterials and Interfaces* 122(30):17347–57. doi: 10.1021/acs.jpcc.8b05416.

Della Rocca, Joseph, Demin Liu, and Wenbin Lin. 2011. 'Nanoscale Metal-Organic Frameworks for Biomedical Imaging and Drug Delivery'. *Accounts of Chemical Research* 44(10):957–68. doi: 10.1021/ar200028a.

Elsaidi, Sameh K., Daniele Ongari, Wenqian Xu, Mona H. Mohamed, Maciej Haranczyk, and Praveen K. Thallapally. 2017. 'Xenon Recovery at Room Temperature Using Metal-Organic Frameworks'. *Chemistry-A European Journal* 23(45):10758. Retrieved 27 December 2020 (http://infoscience.epfl.ch/record/230534).

Erucar, Ilknur, and Seda Keskin. 2016. 'Efficient Storage of Drug and Cosmetic Molecules in Biocompatible Metal Organic Frameworks: A Molecular Simulation Study'. *Industrial & Engineering Chemistry Research* 55(7):1929–39. doi: 10.1021/acs.iecr.5b04556.

Franks, N. P., R. Dickinson, S. L. M. de Sousa, A. C. Hall, and W. R. Lieb. 1998. 'How Does Xenon Produce Anaesthesia?' *Nature* 396(6709):324–324. doi: 10.1038/24525.

Goedecker, S., M. Teter, and J. Hutter. 1996. 'Separable Dual-Space Gaussian Pseudopotentials'. *Physical Review B* 54(3):1703–10. doi: 10.1103/PhysRevB.54.1703.

Goto, Takahisa. 2002. 'Is There a Future for Xenon Anesthesia?' *Canadian Journal of Anesthesia* 49(4):335–38. doi: 10.1007/BF03017319.

Grimme, Stefan, Jens Antony, Stephan Ehrlich, and Helge Krieg. 2010. 'A Consistent and Accurate Ab Initio Parametrization of Density Functional Dispersion Correction (DFT-D) for the 94 Elements H-Pu'. *The Journal of Chemical Physics* 132(15):154104. doi: 10.1063/1.3382344.

Groom, Colin R., and Frank H. Allen. 2014. 'ChemInform Abstract: The Cambridge Structural Database in Retrospect and Prospect'. *ChemInform* 45(17). doi: 10.1002/chin.201417294.

Gulcay, Ezgi, and Ilknur Erucar. 2019. 'Biocompatible MOFs for Storage and Separation of O2: A Molecular Simulation Study'. *Industrial & Engineering Chemistry Research* 58(8):3225–37. doi: 10.1021/acs.iecr.8b04084.

Gurdal, Yeliz, and Seda Keskin. 2012. 'Atomically Detailed Modeling of Metal Organic Frameworks for Adsorption, Diffusion, and Separation of Noble Gas Mixtures'. *Industrial & Engineering Chemistry Research* 51(21):7373–82. doi: 10.1021/ie300766s.

Huang, HongCai Yong-Liang, and Dan Li. 2019. ‘Biological Metal–Organic Frameworks: Structures, Host–Guest Chemistry and Bio-Applications - ScienceDirect’. Retrieved 14 July 2022 (https://www.sciencedirect.com/science/article/abs/pii/S0010854517304538).

Ilknur Erucar, Seda Keskin. 2016. ‘Computational Assessment of MOF Membranes for CH4/H2 Separations - ScienceDirect’. Retrieved 12 July 2022 (https://www.sciencedirect.com/science/article/abs/pii/S0376738816303118).

Imaz, Inhar, Marta Rubio-Martínez, Jihyun An, Isabel Solé-Font, Nathaniel L. Rosi, and Daniel Maspoch. 2011. ‘Metal–Biomolecule Frameworks (MBioFs)’. *Chemical Communications* 47(26):7287–7302. doi: 10.1039/C1CC11202C.

Lagorsse, S., Fernão Magalhães, and Adélio Mendes. 2007. ‘Xenon Recycling in an Anaesthetic Closed-System Using Carbon Molecular Sieve Membranes’. *Journal of Membrane Science* 301:29–38. doi: 10.1016/j.memsci.2007.05.032.

Li, Hailian, M. Eddaoudi, M. O’keeffe, and O. Yaghi. 1999. ‘Design and Synthesis of an Exceptionally Stable and Highly Porous Metal-Organic Framework’. *Nature*. doi: 10.1038/46248.

Li, Jian-Rong, Julian Sculley, and Hong-Cai Zhou. 2012. ‘Metal-Organic Frameworks for Separations’. *Chemical Reviews* 112(2):869–932. doi: 10.1021/cr200190s.

Liu, Jiang-Hua, Chun-Yuan Chen, Zheng-Zhao Liu, Zhong-Wei Luo, Shan-Shan Rao, Ling Jin, Teng-Fei Wan, Tao Yue, Yi-Juan Tan, Hao Yin, Fei Yang, Fei-Yu Huang, Jian Guo, Yi-Yi Wang, Kun Xia, Jia Cao, Zhen-Xing Wang, Chun-Gu Hong, Ming-Jie Luo, Xiong-Ke Hu, Yi-Wei Liu, Wei Du, Juan Luo, Yin Hu, Yan Zhang, Jie Huang, Hong-Ming Li, Ben Wu, Hao-Ming Liu, Tuan-Hui Chen, Yu-Xuan Qian, You-You Li, Shi-Kai Feng, Yang Chen, Lu-Yue Qi, Ran Xu, Si-Yuan Tang, and Hui Xie. 2021. ‘Extracellular Vesicles from Child Gut Microbiota Enter into Bone to Preserve Bone Mass and Strength’. *Advanced Science (Weinheim, Baden-Wurttemberg, Germany)* 8(9):2004831. doi: 10.1002/advs.202004831.

Ljubojev, Nadezda, Marijana Dukić Mijatović, and Željko Bjelajac. 2017. ‘Legal Protection from Climate Change in the Republic of Serbia in the Process of Integration to the European Union’. *Oxidation Communications* 40:1392–1403.

Lynch, Carl, Jan Baum, Rob Tenbrinck, and Richard B. Weiskopf. 2000. ‘Xenon Anesthesia’. *Anesthesiology* 92(3):865–70. doi: 10.1097/00000542-200003000-00031.

Ma, Shengqian, and Hong-Cai Zhou. 2010. ‘Gas Storage in Porous Metal-Organic Frameworks for Clean Energy Applications’. *Chemical Communications (Cambridge, England)* 46(1):44–53. doi: 10.1039/b916295j.

Macrae, Clare F., Ioana Sovago, Simon J. Cottrell, Peter T. A. Galek, Patrick McCabe, Elna Pidcock, Michael Platings, Greg P. Shields, Joanna S. Stevens, Matthew Towler, and Peter A. Wood. 2020. ‘Mercury 4.0: From Visualization to Analysis, Design and

Prediction'. *Journal of Applied Crystallography* 53(Pt 1):226–35. doi: 10.1107/S1600576719014092.

Manz, Thomas A. 2017. 'Introducing DDEC6 Atomic Population Analysis: Part 3. Comprehensive Method to Compute Bond Orders'. *RSC Advances* 7(72):45552–81. doi: 10.1039/C7RA07400J.

McKinlay, Alistair C., Russell E. Morris, Patricia Horcajada, Gérard Férey, Ruxandra Gref, Patrick Couvreur, and Christian Serre. 2010. 'BioMOFs: Metal-Organic Frameworks for Biological and Medical Applications'. *Angewandte Chemie (International Ed. in English)* 49(36):6260–66. doi: 10.1002/anie.201000048.

Meenakshi Dutt, Olga Kuksenok. 2011. 'Modeling the Self-Assembly of Lipids and Nanotubes in Solution: Forming Vesicles and Bicelles with Transmembrane Nanotube Channels | ACS Nano'. Retrieved 15 July 2022 (https://pubs.acs.org/doi/10.1021/nn201260r).

Mehmet Emin ORHAN. 2008. 'Anestezi Dergisi'. Retrieved 13 July 2022 (https://anestezidergisi.com/cilt/16/sayi/3).

Nickalls, R. W. D., and W. W. Mapleson. 2003. 'Age-Related Iso-MAC Charts for Isoflurane, Sevoflurane and Desflurane in Man †'. *British Journal of Anaesthesia* 91(2):170–74. doi: 10.1093/bja/aeg132.

Orhan, Mehmet Emin. 2008. 'ANESTEZİDE XENON: GEÇMİŞ VE GÜNÜMÜZ'. 5.

Perdew, null, null Burke, and null Ernzerhof. 1996. 'Generalized Gradient Approximation Made Simple'. *Physical Review Letters* 77(18):3865–68. doi: 10.1103/PhysRevLett.77.3865.

Perez-Carbajo, Julio, Ismael Matito-Martos, Salvador R. G. Balestra, Mihalis N. Tsampas, Mauritius C. M. van de Sanden, José A. Delgado, V. Ismael Águeda, Patrick J. Merkling, and Sofia Calero. 2018. 'Zeolites for CO2-CO-O2 Separation to Obtain CO2-Neutral Fuels'. *ACS Applied Materials & Interfaces* 10(24):20512–20. doi: 10.1021/acsami.8b04507.

Rae, Ian D. 2016. 'Theory versus Practice in the Twentieth-Century Search for the Ideal Anaesthetic Gas'. *Ambix* 63(1):46–65. doi: 10.1080/00026980.2016.1163638.

Randall Q. Snurr, Yongchul G. Chung. 2019. 'Advances, Updates, and Analytics for the Computation-Ready, Experimental Metal-Organic Framework Database: CoRE MOF 2019'. *Northwestern Scholars*. Retrieved 14 July 2022 (https://www.scholars.northwestern.edu/en/publications/advances-updates-and-analytics-for-the-computation-ready-experime/fingerprints/).

Ryan, Susan M., and Claus J. Nielsen. 2010. 'Global Warming Potential of Inhaled Anesthetics: Application to Clinical Use'. *Anesthesia and Analgesia* 111(1):92–98. doi: 10.1213/ANE.0b013e3181e058d7.

Sanders, R. D., N. P. Franks, and M. Maze. 2003. ‘Xenon: No Stranger to Anaesthesia’. *British Journal of Anaesthesia* 91(5):709–17. doi: 10.1093/bja/aeg232.

Seda Keskin. 2011. ‘Adsorption, Diffusion, and Separation of CH4/H2 Mixtures in Covalent Organic Frameworks: Molecular Simulations and Theoretical Predictions | The Journal of Physical Chemistry C’. Retrieved 15 July 2022 (https://pubs.acs.org/doi/abs/10.1021/jp209804x).

Stanley, Theodore H. 2000. ‘Anesthesia for the 21st Century’. *Baylor University Medical Center Proceedings* 13(1):7–10. doi: 10.1080/08998280.2000.11927635.

Sumida, Kenji, David L. Rogow, Jarad A. Mason, Thomas M. McDonald, Eric D. Bloch, Zoey R. Herm, Tae-Hyun Bae, and Jeffrey R. Long. 2012. ‘Carbon Dioxide Capture in Metal-Organic Frameworks’. *Chemical Reviews* 112(2):724–81. doi: 10.1021/cr2003272.

Sumit Sharma. 2019. ‘Molecular Dynamics Simulation of Nanocomposites Using BIOVIA Materials Studio, Lammps and Gromacs | ScienceDirect’. Retrieved 15 July 2022 (https://www.sciencedirect.com/book/9780128169544/molecular-dynamics-simulation-of-nanocomposites-using-biovia-materials-studio-lammps-and-gromacs).

Tamames-Tabar, A. García-Márquez C. 2014. ‘MOFs in Pharmaceutical Technology - Bio- and Bioinspired Nanomaterials - Wiley Online Library’. Retrieved 12 July 2022 (https://onlinelibrary.wiley.com/doi/abs/10.1002/9783527675821.ch04).

Ullmann, Fritz. 2003. *Ullmann’s Encyclopedia of Industrial Chemistry*. Wiley-VCH.

VandeVondele, Joost, and Jürg Hutter. 2007. ‘Gaussian Basis Sets for Accurate Calculations on Molecular Systems in Gas and Condensed Phases’. *The Journal of Chemical Physics* 127(11):114105. doi: 10.1063/1.2770708.

Verlet, Loup. 1967. ‘Computer “Experiments” on Classical Fluids. I. Thermodynamical Properties of Lennard-Jones Molecules’. *Physical Review* 159(1):98–103. doi: 10.1103/PhysRev.159.98.

Yaghi, Omar M., Michael O’Keeffe, Nathan W. Ockwig, Hee K. Chae, Mohamed Eddaoudi, and Jaheon Kim. 2003. ‘Reticular Synthesis and the Design of New Materials’. *Nature* 423(6941):705–14. doi: 10.1038/nature01650.

APPENDİX

Appendix A

Appendix A1. Structural parameters of the Bio-MOFs under consideration

Table A1. LCD stands for the largest cavity diameter in Å, PLD is pore limiting diameter in Å, and SA is surface area in m^2/g. PLD and LCD are defined as the smallest opening along the pore and the largest size of the included sphere that can fit to the pores, respectively. For more detailed information we refer reader to the MOFDB API Database or to t**he Cambridge Crystallographic Data Centre (CCDC).**

MOF Names	Biomolecules	Metal Sites	LCD (Å)	PLD (Å)	Void Fraction	SA(m^2 /g)
BIPSUQ	Porphyrin	Cu	18.61	16.93	0.83	4502.66
BEWCUD	Porphyrin	Zn	10.59	8.54	0.81	4454.34
ADUWON	Formadide	Ni	16.38	6	0.78	4298.28
ZEZFIV	Formadide	Na, Zn	10.69	9.42	0.74	3541.03
ADASOP	Formadide	Zn	18.04	6.69	0.83	3346.21
AGOFEJ	Formadide	Cu	12.61	8.72	0.76	3269.05
BEDYEQ	Porphyrin	Zr	32.02	31	0.86	2737.39
ADUWIH	Formadide	Zn	9.28	6.55	0.72	2605.83
DUPVER	Adenine	Zn	9.93	6.47	0.73	2595.58
LONWIW	Formadide	Mg	6.33	5.31	0.66	2526
RUGKOV	Adenine	Zn	6.88	5.43	0.69	2525.58
ZUGDEM	Adenine	Zn	9.67	5.99	0.69	2360.71
FIQCEN	Tricarboxylate	Cu	13.19	6.67	0.76	2132.15
IVILEG	Adenine	Zn	14.15	13.27	0.72	2021.31
VAGTAA	Formadide	Mg	5.69	4.4	0.59	1703.3
ACIBOE	Formadide	Zn	8.26	7.04	0.62	1609.46
AFUKET	Formadide	Mn	5.97	4.78	0.55	1468.14
WURKEB	Formadide	Mn	6.33	4.86	0.63	1463.97
DUBWON	Formate	Zn	5.41	4.74	0.57	1224.95
CETHEQ	Formate	Cu	8.75	7.35	0.58	1217.73
EZOFEF	Formadide	Ni	11.24	4.57	0.64	1161.91
NUDLAA	Adenine	Zn	10.11	9.13	0.58	1069.49
BEPPAP	Amino	Zn	9.89	9.78	0.43	1029.42
BEYSEF	Adenine	Co	5.62	4.75	0.40	1020.51
BEPLUF	Amino	Zn	9.84	9.74	0.56	960.82
LUSHOX04	Formadide	Mn	5.43	4.96	0.54	909.61
BEPNOB	Amino	Zn	9.66	9.56	0.55	899.02

BEPMAM	Amino	Zn	9.65	9.57	0.55	898.91
LIXWAR	Formadide	Mn	5.6	3.91	0.53	883.22
BEPNUH	Amino	Zn	10.31	10.21	0.47	864.84
LUSHOX	Formadide	Mn	5.31	4.92	0.50	864.79
LUSHOX02	Formadide	Mn	5.4	4.93	0.51	859.89
LUSHOX01	Formadide	Mn	5.26	4.89	0.49	833.1
LUSHOX03	Formadide	Mn	5.24	4.88	0.52	823.97
BEPPOD	Amino	Zn	9.62	9.5	0.49	796.08
IZUMUM	Adenine	Cu	5.58	4.65	0.38	756.79
DOMKEX	Porphyrin	Na	6.2	5.2	0.43	730.1
ADAXIO	Formadide	Co	5.73	5.01	0.49	724.96
XACZEH	Adenine	Cu	10.61	7.24	0.59	720.8
QOHTUD	Muconate	Co	6.67	5.81	0.49	694.26
BEPNIV	Amino	Zn	8.14	8.04	0.64	687.54
BEPPIX	Amino	Zn	7.72	7.6	0.59	630.17
CAYYEG	Porphyrin	Mn	7.23	5.23	0.48	544.7
XILVIZ	Metalloporphyrin	Zn	5.53	4.18	0.64	543.39